Metabolic basis for the evolution of a common pathogenic *Pseudomonas aeruginosa* variant

Dallas L Mould[1], Mirjana Stevanovic[1], Alix Ashare[1,2], Daniel Schultz[1], Deborah A Hogan[1]*

[1]Department of Microbiology and Immunology, Geisel School of Medicine at Dartmouth, Hanover, United States; [2]Department of Medicine, Dartmouth-Hitchock Medical Center, Lebanon, United States

Abstract Microbes frequently evolve in reproducible ways. Here, we show that differences in specific metabolic regulation rather than inter-strain interactions explain the frequent presence of *lasR* loss-of-function (LOF) mutations in the bacterial pathogen *Pseudomonas aeruginosa*. While LasR contributes to virulence through its role in quorum sensing, *lasR* mutants have been associated with more severe disease. A model based on the intrinsic growth kinetics for a wild type strain and its LasR⁻ derivative, in combination with an experimental evolution based genetic screen and further genetics analyses, indicated that differences in metabolism were sufficient to explain the rise of these common mutant types. The evolution of LasR⁻ lineages in laboratory and clinical isolates depended on activity of the two-component system CbrAB, which modulates substrate prioritization through the catabolite repression control pathway. LasR⁻ lineages frequently arise in cystic fibrosis lung infections and their detection correlates with disease severity. Our analysis of bronchoalveolar lavage fluid metabolomes identified compounds that negatively correlate with lung function, and we show that these compounds support enhanced growth of LasR⁻ cells in a CbrB-controlled manner. We propose that in vivo metabolomes contribute to pathogen evolution, which may influence the progression of disease and its treatment.

*For correspondence:
dhogan@dartmouth.edu

Editor's evaluation

This study aimed to identify the genetic foundation favoring selection of lasR mutants in laboratory and clinical isolates from persons with CF. They selected these mutants using a predictable and quantitative framework of evolution experiments and then identified their genetic underpinnings by a suppressor screen. The role of cbrAB as a key intermediate is important and ties together several reports of nutrient-dependent advantages of lasR, including those that may explain their adaptation to conditions found in the CF airway.

Introduction

Quorum sensing (QS) is a mechanism of microbial communication that regulates the expression of a suite of genes in response to diffusible autoinducers in a population (*Schuster and Greenberg, 2007*; *Schuster et al., 2003*). Despite the importance of cell-cell communication for virulence (*Rumbaugh et al., 2009*) and high conservation across divergent phylogenies, key QS regulators in diverse species, such as *Pseudomonas aeruginosa*, *Vibrio cholerae*, and *Staphylococcus aureus*, frequently lose function (*Mould and Hogan, 2021*), due to recent missense and nonsense mutations, indels, or genome

eLife digest Bacteria can evolve quickly, a skill that proves useful in ever-changing environments. For example, individuals in many bacterial species can start to work together under certain circumstances; this ability is underpinned by a system called quorum sensing, which allows cells to detect nearby conspecifics. However, species of harmful bacteria often lose their quorum sensing abilities when they infect humans. This is the case for *Pseudomonas aeruginosa*, which normally lives in the soil but can also cause deadly conditions, especially in hospital settings.

Patients often carry *P. aeruginosa* with mutations that disable the quorum-sensing signal receptor LasR, a molecular actor that can switch on many other genes in a cell. People who are infected with *P. aeruginosa* strains carrying a damaged version of the *lasR* gene are typically more ill and less likely to recover. Why this is the case – and in fact, why genes associated with quorum sensing often lose function during infection – is still unclear.

To investigate this question, Mould et al. used laboratory evolution experiments and computer models of *P. aeruginosa* growth to understand how *lasR* mutant cells evolve. Differences in growth rates and ways to use resources (rather than changes in cell-to-cell interactions) best explained why *lasR* mutants become more successful. Further experiments narrowed down the molecular cascade required for the rise of *lasR* mutants, identifying a pathway that regulates how *P. aeruginosa* switches between different nutrient sources.

This work reveals a new connection between quorum sensing genes and nutrient regulation in bacterial cells. Loss of functional LasR changes the way that cells use nutrients, and thus will reshape how they interact with host cells and other bacteria. This insight could lead to better ways to predict the outcomes of bacterial infections and how to best treat them.

rearrangements. These paradoxical findings suggest that there may be connections between QS and other key physiological pathways that have yet to be revealed.

In *P. aeruginosa*, many isolates from humans, plants, and water sources have loss-of-function mutations in the gene encoding the transcription factor LasR (*Groleau et al., 2022*; *O'Connor et al., 2021*), which is central to an interconnected QS network (*Schuster et al., 2003*). LasR⁻ isolates have been repeatedly observed in *P. aeruginosa* lung infections in people with cystic fibrosis (pwCF) (*Smith et al., 2006*), and LasR⁻ isolate detection is associated with more rapid lung function decline and more inflammation than in comparator populations (*Hoffman et al., 2009*; *LaFayette et al., 2015*). In a clinical study of acute corneal infections (*Hammond et al., 2016*), LasR⁻ strains also correlated with more damage and worse outcomes.

Multiple studies contribute to our understanding of the physiologies and social interactions that impact LasR LOF mutant fitness. Several studies provide evidence in support of the model that LasR⁻ strains are 'social cheaters' that reap the benefits of shared goods secreted by neighboring wild-type cells without incurring the metabolic costs (*Sandoz et al., 2007*). In this case, LasR⁻ strains grow better when the wild type is in the majority, and crash when a critical threshold of LasR⁻ cells is surpassed due to insufficient wild-type support (*West et al., 2006*). The extent of *lasR* mutant 'cheating' depends on the cost-benefit difference, and multiple shared goods, including siderophores, must be considered (*Ozkaya et al., 2018*). To combat the rise of cheaters, *P. aeruginosa* produces products such as hydrogen cyanide, rhamnolipids, or pyocyanin that inhibit the growth of quorum sensing mutants through a process known as 'policing' (*Castañeda-Tamez et al., 2018*; *García-Contreras et al., 2020*; *Wang et al., 2015*). There is evidence that the presence of LasR⁻ subpopulations may be beneficial (*García-Contreras and Loarca, 2020*) and lead to emergent properties including metabolite-driven interactions between wild type and *lasR* mutants that provoke the production of QS-controlled factors by the *lasR* mutant to levels greater than in wild-type monocultures (*Mould et al., 2020*). In addition to the interactions between LasR⁺ and LasR⁻ cells that influence the fitness and behavior of LasR⁻ strains described above, there are important intrinsic characteristics of LasR⁻ strains including increased Anr-regulated microoxic fitness (*Clay et al., 2020*), resistance to alkaline pH in aerobic conditions (*Heurlier et al., 2005*), and altered metabolism (*D'Argenio et al., 2007*). The metabolic advantages associated with LasR⁻ strains include growth on individual amino acids (*D'Argenio et al., 2007*). The numerous differences described between LasR⁺ and LasR⁻ strains indicate that an understanding of the factors

that drive the rise and persistence of *lasR* mutants may be complex and are not yet well understood. While it is clear that there are many ways in which *lasR* LOF mutants differ from their LasR +progenitors, a common trait that promotes the rise of LasR⁻ strains in diverse environments, even in rich and minimal laboratory media (*Heurlier et al., 2005*; *Scribner et al., 2022*; *O Brien et al., 2017*; *Luján et al., 2007*; *Qi et al., 2016*; *Robitaille et al., 2020*; *Sandoz et al., 2007*; *Wong et al., 2012*; *Yan et al., 2018*), has not been established.

Here, we use mathematical modeling, experimental evolution-based genetic screens, phenotype profiling, and whole-genome sequencing of evolved communities in different backgrounds to understand the rise of LasR⁻ strains over only a few serial passages. We identified the CbrAB pathway as the strongest contributor to the rise of *lasR* LOF mutants, and our findings were not specific to strain background or medium. LasR⁻ strains are more commonly detected in samples from individuals with more severe CF lung disease (*Smith et al., 2006*). Analysis of bronchoalveolar lavage samples from pwCF and non-CF comparators identified several compounds that were higher in pwCF and that inversely correlated with lung function. LasR⁻ strains showed improved growth on the majority of these compounds, many of which were amino acids, and epistasis analysis confirmed that the improved growth was due to altered activity of the CbrB-CrcZ-Crc pathway.

Results
Mathematical model built from monoculture growth data predicts the observed rise of *lasR* loss-of-function mutants

Our previous work on microbial interactions involving LasR⁺ and LasR⁻ *P. aeruginosa* revealed subtle differences in growth kinetics (*Mould et al., 2020*). In monoculture, *P. aeruginosa* strain PA14 Δ*lasR* had no lag phase, while the wild type had a lag phase of 1 h (*Figure 1A* for summary data and *Figure 1—figure supplement 1* for growth curve). Furthermore, consistent with work by others, the Δ*lasR* strain had a lower growth rate (*García-Contreras et al., 2020*) but a 1.5-fold higher yield in LB (*Diggle et al., 2007*). We found no differences in death rate resulting from elevated culture pH (as has previously been reported in low oxygen conditions [*Heurlier et al., 2005*]) or the onset of death phase relative to PA14 wild type under these conditions (*Figure 1—figure supplement 1*).

We built a mathematical model of strain competition exclusively from experimentally determined monoculture growth parameters to predict the relative changes in wild type and LasR⁻ cell numbers when grown on a common pool of growth substrates in order to determine how differences in growth kinetics alone would impact the rise of LasR⁻ lineages (*Figure 1A*). We modeled cell density (*Figure 1A* -left y-axis) and the percentage of LasR⁻ cells (*Figure 1A* -right y-axis) assuming a shared nutrient source and a passage every 48 hr which is a regime used previously to study the selection for LasR⁻ cells (*Heurlier et al., 2005*). Based on the mutation frequency of the *P. aeruginosa* strain PA14 (0.52×10^{-3} per genome per generation) (*Dettman et al., 2016*) and the size of the *lasR* gene (720 bp) relative to the genome (~ 6 Mbp), we approximate 50 *lasR* alleles with nucleotide changes would be present in a dense culture (~ 10^8 cells), a fraction of which would lead to a LasR⁻ phenotype. With the assumption of 2 to 20 LasR⁻ cells per inoculum (t = 0, ~ 10^5 cells), the model predicted that ~ 20% of the population would consist of LasR⁻ cells by Day 4, with increased percentages of ~ 40% and ~ 80% by Days 6 and 8, respectively (*Figure 1A*). Only minor differences in percentages resulted from changes in the initial LasR⁻ population.

We compared the model output to experimental data gathered with the same growth conditions and evolution regime. A single PA14 wild-type colony was used to inoculate a 5 mL culture of LB, which was grown to saturation and then used to inoculate three 5 mL LB cultures which were then passaged independently. Results from all three replicates from four independent experiments are shown. The percent of cells with LOF phenotypes were enumerated by plating and determining the percent of colonies with the characteristic 'sheen' colony morphology of LasR⁻ cells that result from accumulation of 4-hydroxy-2-heptylquinoline (HHQ) (*Figure 1B*; *D'Argenio et al., 2007*). In all four independent experiments, the percentage of colonies with the LasR⁻ phenotype rose from undetectable levels to an average of ~ 80% over the course of 8 days (*Figure 1B*). To validate the use of colony sheen as an indicator of the LasR⁻ genotype, we evaluated ≥ 90 isolates with the characteristic LasR⁻ colony morphology for other phenotypes associated with LOF: low production of proteases and autoinducers (3OC12HSL and C4HSL). Most of the predicted LasR⁻ isolates (~ 90%) had phenotypes
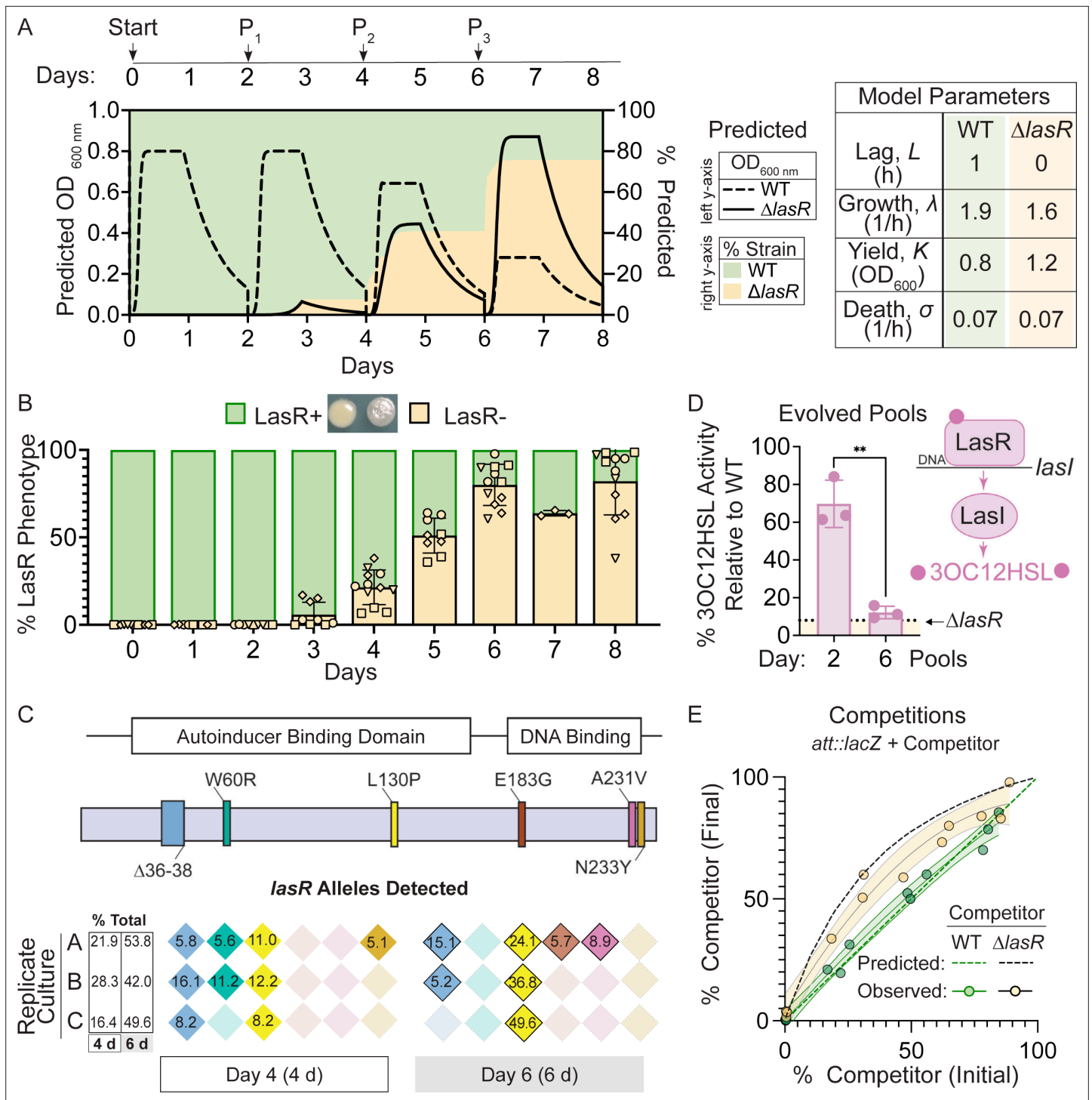
Figure 1. Mathematical model built from monoculture growth data is sufficient to explain the rise of LasR loss-of-function strains. (**A**) Predicted densities (left y-axis) of mathematical model shown for wild type (WT, dashed line) and LasR⁻ (solid line) strains. Predicted percentages (right y-axis) of LasR⁻ (beige fill) and LasR+ (green fill) strains over the course of evolution regime in LB with passage (P_n) every 2 days. Table shows experimentally measured growth parameters used to create the model as obtained for strains PA14 WT and $\Delta lasR$ grown in 5 mL LB cultures on a roller drum. (**B**) Percentage of LasR⁻ phenotypes observed in $n \geq 4$ independent evolution experiments in LB. Different shapes represent independent experiments, and same shapes represent technical replicates. A representative image of the smooth LasR+ and sheen LasR⁻ colonies from Day 6 is shown. (**C**) *lasR* alleles detected in the population at Day 4 (4 d) and Day 6 (6 d) by PoolSeq within the *lasR* coding sequence, which includes the autoinducer binding and DNA binding domains, for a representative experiment (diamond symbols, in B). The percentages of each allele and the sum (i.e. % total) is indicated for each replicate culture. Each color represents a different allele. (**D**) LasR regulates the production of its cognate autoinducer 3OC12HSL via direct

Figure 1 continued on next page

Figure 1 continued

transcriptional control of the gene encoding the LasI synthase. LasI-produced autoinducer activity of evolved pools from a representative experiment (diamond symbols, in B) at days 2 and 6. Activity is presented as a percentage of that produced by unevolved WT monocultures. The levels produced by the engineered Δ*lasR* control strain is shown for reference (dotted line). **, p = 0.0015 as determined by two-tailed, upaired t-test. (**E**) Comparison of predicted (dashed line) and observed (solid line) outcomes of competition assays initiated at different initial ratios for which a constitutively tagged WT (*att::lacZ*) was competed against Δ*lasR* (beige, gray line) or WT (control, green) competitors for 6 h (final) in planktonic LB cultures with 95% confidence intervals shown for best fit line (quadratic).

The online version of this article includes the following figure supplement(s) for figure 1:

Figure supplement 1. Experimentally determined growth parameters of PA14 wild type and Δ*lasR* monocultures in LB.

Figure supplement 2. Phenotype analysis of sheen LasR⁻ candidates isolated from the evolution experiments in LB.

that mirrored those of the PA14 Δ*lasR* strain, and not wild type (*Figure 1—figure supplement 2*). Consistent with other studies (*Feltner et al., 2016*), approximately 15% of the cells with other LasR⁻ phenotypes produced high levels of C4HSL even though 3OC12HSL production was low.

The percentage of LasR⁻ cells predicted by the model matched the frequency of *lasR* alleles in genome sequence data from pools of colonies obtained from Day 4 and 6 cultures of a representative experiment (diamond symbols in *Figure 1B*). Across replicates, six non-synonymous mutations were identified in *lasR* in the regions corresponding to the LasR autoinducer binding (Δ36–38, W60R, and L130P) and DNA binding domains (E183G, A231V, and N233Y) (*Figure 1C* and *Supplementary file 1*), which are important for function (*Feltner et al., 2016*). No synonymous mutations in *lasR* were detected. Two mutations (Δ36–38 and L130P) were present in all three replicate cultures at Day 4 and thus were likely present in the initial inoculum. In replicate A, two additional mutations in *lasR* (E183G and A231V) were identified at Day 6; the LasR A231V substitution has been extensively characterized as a loss-of-function mutation through phenotyping and genetic complementation (*Luján et al., 2007*; *Qi et al., 2016*). The percentage of *lasR* mutants in the evolved population detected by sequencing at Day 4 (22.2 ± 6.0% s.d.) and Day 6 (48.5 ± 4.9% s.d.) (*Figure 1C*) closely resembled the percentage of LasR⁻ strains predicted by the model (~ 20% and ~ 50%, respectively) (*Figure 1A*). The increased frequency of cells with the allele encoding the L130P substitution (*McCready et al., 2019*) between Day 4 and Day 6, with 13.1%, 24.6%, and 41.4% increases in replicate cultures, suggests strong selection for this particular variant or the presence of an additional mutation(s) in this background. In support of the significant increases in LasR⁻ subpopulations, the evolved cultures themselves had lower levels of the LasR-regulated autoinducer 3OC12HSL; by Day 2, culture 3OC12HSL levels were ~ 30% lower than a non-evolved wild-type culture, and showed a ~ 90% reduction by Day 6 (*Figure 1D*).

To further test the predictive power of our model for the rise of LasR⁻ lineages, we initiated cultures with different ratios of a constitutively tagged wild type (*att::lacZ*) against untagged wild-type or Δ*lasR* mutant competitors. A control assay demonstrated that the ratios of tagged and untagged wild type were unchanged over the course of growth, as indicated previously under distinct conditions (*Clay et al., 2020*; *Mould et al., 2020*). When the Δ*lasR* competitor was cultured with the tagged wild type for 6 hr, the percentage of Δ*lasR* mutant cells in the total population increased regardless of the initial percentage of Δ*lasR* (1–85%) at the time of inoculation (*Figure 1E*). The model successfully predicted that Δ*lasR* would outcompete the wild type over this range which is consistent with differential growth kinetics playing a major role (*Figure 1E* -dotted line). No Δ*lasR* advantage would be observed when it is at high initial percentages if its advantage was solely due to exploitation of common goods, as is observed when WT and Δ*lasR* are co-cultured on a substrate that requires WT protease production (*Sandoz et al., 2007*). There were differences between the best fit lines for the actual and predicted data that could be due to a variety of factors including measurement error or biological interactions between WT and Δ*lasR* strains (e.g policing *Castañeda-Tamez et al., 2018*; *Wang et al., 2015*).

Activity of CbrAB, the two-component system that regulates carbon utilization, is required for the rise of LasR⁻ strains

To test which genes or pathways were required to promote the selection of LasR⁻ cells, we applied reverse genetics to experimental evolution. In *P. aeruginosa,* the sensor kinases of two-component systems, encoded throughout the genome, respond to a variety of diverse internal and environmental cues, such as nutrient limitation or stresses, that may be relevant to differential fitness (*Rodrigue*

et al., 2000; *Wang et al., 2021*). Using a library of 63 sensor kinase deletion mutants (*Wang et al., 2021*), we screened each mutant for the rise of LasR⁻ phenotypes in triplicate in a 96-well plate format (*Figure 2—figure supplement 1*). In the primary microtiter dish-based screen, in which the investigators were blind to mutant strain identity, five gene knock-outs (Δ*cbrA*, Δ*gacS*, Δ*fleS*, ΔPA14_64580, and ΔPA14_10770) showed no detectable 'sheen' colony phenotypes characteristic of LasR⁻ strains in any of the three replicates (*Figure 2—figure supplement 1* & *Supplementary file 2*). In a secondary screen of these five mutants in five mL cultures, only the Δ*cbrA* mutant (*Figure 2A*) did not evolve LasR⁻ phenotypes after serial passage; the other four mutants all had significant subpopulations with LasR⁻ phenotypes by Day 6 (*Figure 2—figure supplement 2A*). LasR⁻ strains rose with a similar frequency as in the wild type progenitor when evolution experiments were initiated with strains lacking the regulator Anr, important for LasR⁻ microoxic fitness, or the regulator RhlR, important for *lasR* mutant policing (*Chen et al., 2019*; *Clay et al., 2020*) suggesting that these regulators were not major contributors to fitness under these conditions (*Figure 2—figure supplement 2B*).

CbrA, through its regulation of the response regulator CbrB, (*D'Argenio et al., 2007*; *Sonnleitner et al., 2009*), controls *P. aeruginosa* preferential catabolism of certain carbon sources, such as succinate, over others (e.g. amino acids) through a process referred to as catabolite repression. In support of the finding that CbrA was essential for the evolution of LasR⁻ lineages, the Δ*cbrB* mutant also showed a striking and significant reduction in LasR⁻ phenotypes over the course of 8 days (*Figure 2A*). Additionally, evolution experiments in a LasR⁺ cystic fibrosis clinical isolate (DH2417) showed a similar rise in LasR⁻ phenotypes over the course of evolution, which was delayed and reduced in a Δ*cbrB* derivative (*Figure 2A*). CbrAB-controlled catabolite repression is regulated by Crc, in complex with the RNA-binding protein Hfq, which together repress the translation of target mRNAs involved in the transport and catabolism of less preferred substrates (*Figure 2B*; *Sonnleitner et al., 2017*). Crc activity is down regulated by the small RNA *crcZ*, which sequesters Crc away from its mRNA targets. The CbrAB two-component system transcriptionally regulates levels of *crcZ* (*Figure 2B*; *Sonnleitner et al., 2009*) in response to signals that have yet to be described.

Consistent with the absence of LasR⁻ phenotypes in evolved Δ*cbrA* or Δ*cbrB* cultures, Pool-Seq analysis found no mutations in *lasR* on either Day 4 or 6 (*Figure 2C*, pink and *Supplementary file 1*) which was in striking contrast to the multiple LasR⁻ alleles observed in wild type cultures. The absence of *lasR* mutations in the Δ*cbrA* and Δ*cbrB* derivatives was not due to differences in mutation frequency or number of generations as other mutations in distinct pathways under selection (e.g. *fleR* in *Figure 2C*) were present at comparable levels in all cultures (*Supplementary file 1* for data). In addition, strain PA14 wild type and the Δ*cbrA* mutant had similar growth patterns as assessed by daily optical density measurements (*Figure 2—figure supplement 2C*). We also assessed a number of factors other than differential growth that could affect the rise of LasR⁻ lineages. A previous report *Heurlier et al., 2005* found that LasR⁻ strains in the PAO1 background undergo less severe alkaline-induced lysis in another complex medium (nutrient yeast broth) when grown aerobically, but we found no evidence of differential lysis in LB between wild-type and Δ*lasR* strains under our conditions (*Figure 1—figure supplement 1A*). Furthermore, buffering the medium to pH 7 suppressed medium alkalinization (from pH of 6.8–8.5) and lysis (*Crocker et al., 2019*), but not the rise of LasR⁻ lineages; though, the kinetics of LasR⁻ lineage detection was delayed with buffering (*Figure 2—figure supplement 2D* and *Sandoz et al., 2007*). Lastly, to assess potential differences in toxicity of the wild type and Δ*cbrB* mutant culture supernatants toward LasR⁻ cells through the production of secreted factors (*Yan et al., 2018*), we grew the Δ*lasR* mutant in spent filtrate from wild-type and Δ*cbrB* cultures; no significant differences in colony forming units were observed (*Figure 2—figure supplement 2E*).

The activation of CbrAB increases growth on diverse metabolites by inducing *crcZ* which sequesters Crc away from the targets that it translationally represses (*Figure 2B* for pathway). In D'Argenio et al. (*D'Argenio et al., 2007*), higher CbrB levels were observed in LasR⁻ strains in a proteomics analysis, but no direct interactions between LasR and components of CbrA-CbrB-*crcZ*-Crc pathway have been described. Because CbrA, CbrB, and *crcZ* act to repress Crc, we hypothesized that if the loss of LasR function led to higher activity of the CbrA-CbrB-*crcZ* pathway and less Crc translational repression, we might also observe loss-of-function mutations in the genes encoding Crc or Hfq in the absence of *cbrB* (*Figure 2B*). Interestingly, the pooled genome sequence data from the Day 4 (open symbols) and Day 6 (grey symbols) populations evolved in the Δ*cbrA* and Δ*cbrB* backgrounds identified seven different mutations in *crc*, including three nonsense mutations, four missense mutations,
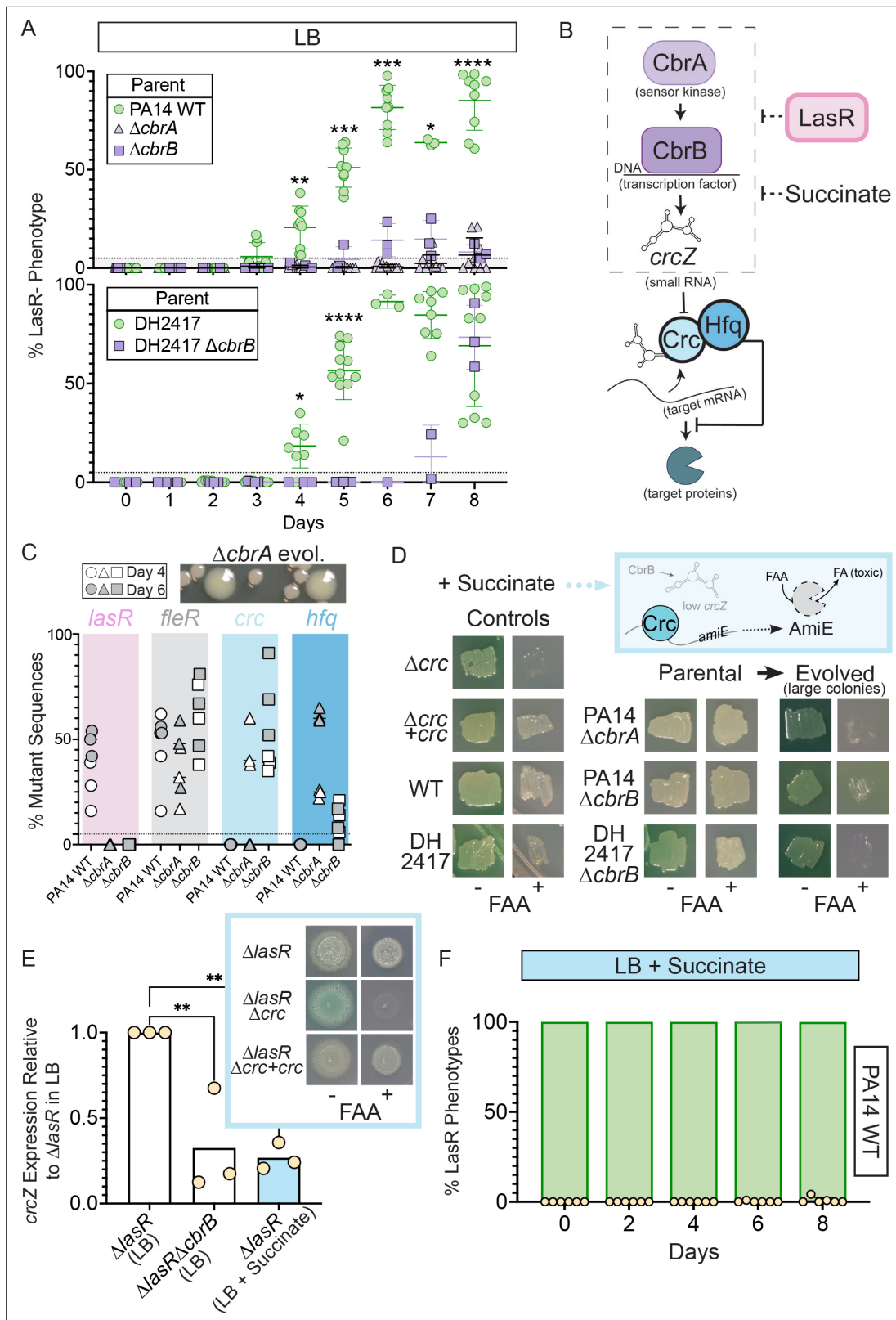
Figure 2. Activity of the carbon catabolite repression system is required for LasR⁻ selection in LB. (**A**) The percentage of colonies with LasR⁻ phenotypes enumerated over the course of evolution for ΔcbrA or ΔcbrB mutants (purple triangle and square, respectively) in strains PA14 or a LasR+ cystic fibrosis isolate (DH2417) relative to 'wild-type' comparators. PA14 WT strain data is the same as in *Figure 1B* (n ≥ 3). Statistical significance was determined between percent LasR⁻ phenotypes in CbrA/B + and *cbrA/B* mutant pools each day via Two-Way ANOVA with Dunnet's multiple hypothesis correction.

Figure 2 continued on next page

Figure 2 continued

For all panels: *, p < 0.05; **, p < 0.005; ***, p < 0.0005; ****, p < 0.0001. (**B**) The carbon catabolite repression system promotes the preferential consumption of succinate (and other preferred substrates) through the two-component system CbrAB. CbrA activates its response regulator CbrB which directly induces expression of the small RNA *crcZ*. *crcZ* sequesters Crc thereby allowing translation of the target gene to occur. Often the target gene enables the utilization of specific (i.e. less preferred) substrates. In a catabolite repressed state, such as when succinate is present, Crc binds to target mRNA with the RNA binding protein Hfq and blocks translation. CbrB protein levels are higher in strains lacking LasR function, but the mechanism linking these pathways is uncharacterized. (**C**) Percent total mutant alleles in *lasR* (pink bar), *fleR* (gray bar), *crc* (light blue bar), and *hfq* (darker blue bar) in a representative experiment (*Figure 1B*, diamond symbols) for PA14 wild type, ΔcbrA, ΔcbrB evolved populations sequenced on Day 4 (white filled symbol) and six (gray filled symbol). Representative image of the larger colony morphologies observed in the evolved pools from CbrA/B- deficient strains (ΔcbrA shown) above. (**D**) Crc represses *amiE* encoding an amidase that can turnover the fluoroacetamide (FAA) protoxin to fluoroacetate (FA) mediating cell death. In the presence of succinate, cells with functional Crc survive in the presence of FAA. PA14 WT, PA14 ΔcbrA, PA14 ΔcbrB, and DH2417 WT strains were included as controls. The ΔcbrA and ΔcbrB parental strains used for the evolution experiments and representative colonies that emerged with a larger colony size in these backgrounds were patched (or struck out) onto succinate containing plates in the absence and presence of the FAA protoxin. (**E**) *crcZ* expression of PA14 ΔlasR in LB (white bar) and LB with 40 mM succinate (blue bar) measured by qRT-PCR and plotted relative to expression of ΔlasR in LB (n = 4). Inset shows representative image of ΔlasR, ΔlasRΔcrc, and ΔlasRΔcrc +crc grown on succinate containing plates in the absence and presence of FAA. (**F**) Percentage of colonies with LasR⁻ phenotypes observed in evolution experiment initiated with strain PA14 WT in LB supplemented with 40 mM succinate (n = 6). P-values of 0.007 and 0.005 for comparison of ΔlasRΔcbrB (LB) and ΔlasR (LB +succinate) relative to ΔlasR grown in LB as determined by ordinary one-way ANOVA with Dunnett's multiple comparison test.

The online version of this article includes the following figure supplement(s) for figure 2:

Figure supplement 1. Screen reveals specific requirement of CbrA, and not other sensor kinases encoded in the PA14 genome for LasR⁻ strain selection.

Figure supplement 2. LasR⁻ strains evolve in all tested strain backgrounds except for those deficient in *cbrAB,* and this is independent of cellular density, lysis, and filtrate toxicity.

and six indels, and these were among the most abundant mutations in the ΔcbrB mutant cultures; no *crc* mutations were identified in the PA14 wild type evolved populations (*Figure 2C*). In ΔcbrB, *crc* mutant alleles showed the largest rise between Day 4 and Day 6 across all three replicate cultures (*Supplementary file 1*). In the ΔcbrA passaged cultures, we also identified a rise in *hfq* mutations within the coding and upstream intergenic regions (*Figure 2C* and *Supplementary file 1* for sequence data) in addition to mutations in *crc*. The changes in relative abundances of alleles with mutations in *crc* and either the promoter or coding regions of *hfq* across the 2 days suggested that *hfq* mutations and *crc* mutations were in different backgrounds (*Supplementary file 1*).

To assess Crc-Hfq function in evolved strains, we leveraged Crc translational repression of the amidase AmiE, which cleaves the prototoxin FAA to the toxic FA (*Figure 2D* for pathway) (*O'Toole et al., 2000*). Succinate, which downregulates CbrAB activity, maintains repression of AmiE, thereby enabling wild type to grow in the presence of FAA. In the absence of functional Crc or its co-repressor Hfq, cells synthesize AmiE, and FAA conversion into FA inhibits growth. As expected, on medium with succinate, FAA inhibited growth of the Δcrc mutant, but did not affect growth of the complemented Δcrc +crc strain, the wild type, and the ΔcbrA and ΔcbrB mutants. However, in passaged ΔcbrA and ΔcbrB cultures, spontaneous mutants in the population gave rise to larger colonies (*Figure 2C*, top), and these isolates were FAA sensitive (*Figure 2D*) supporting the model that in the ΔcbrA and ΔcbrB backgrounds, mutations that abolished Crc or Hfq activity arose. Secondary mutants with FAA sensitivity also arose in the DH2417 ΔcbrB background upon passaging, indicating that this phenomenon was not unique to the PA14 background, and another study also reported *crc* and *hfq* mutants in the absence of *cbrB* (*Boyle et al., 2017*). Given the apparent selection for decreased Crc function in ΔcbrA and ΔcbrB, and the requirement of *cbrA* or *cbrB* for LasR⁻ strain selection, we hypothesized that increased CbrAB activity may be a trait that increases the fitness of LasR⁻ strains.

To complement the genetics approach of evolution assays in *cbrAB* mutants, we monitored the rise of LasR⁻ lineages in LB medium supplemented with succinate, which inhibits CbrAB activity (*Sonnleitner et al., 2009*). Medium amendment with 40 mM (pH 7) succinate was sufficient to repress CbrB-regulated *crcZ* small RNA expression in ΔlasR to levels reminiscent of ΔlasRΔcbrB (*Figure 2D*). *lasR* mutants still responded to succinate; succinate reduced *crcZ* levels in ΔlasR and enabled ΔlasR growth on medium with FAA due to Crc activity (*Figure 2E*, inset). This indicated that ΔlasR retains the Crc-Hfq mediated translational repression when succinate is present. Succinate amendment suppressed the rise of LasR⁻ phenotypes in PA14 wild type (*Figure 2F*).

Elevated *cbrB* and *crcZ* expression and reduced Crc-dependent repression are sufficient to recapitulate the growth advantages of LasR⁻ strains

CbrAB activity induces the expression of *crcZ*, which sequesters Crc. We found that the Δ*lasR* mutant had ~two fold higher *crcZ* levels compared to wild type, suggesting higher activity of the CbrAB two-component system in LasR⁻ strains (*Figure 3A*). Previous work reported higher yields on phenylalanine for LasR⁻ relative to LasR⁺ strains concomitant with elevated CbrB protein levels in a proteomics analysis (*D'Argenio et al., 2007*). Thus, we first used phenylalanine as a growth substrate to further dissect the activity of the CbrAB-*crcZ*-Crc pathway (*Figure 2B* for pathway) in LasR⁻ strains. In planktonic cultures in medium with phenylalanine as a sole carbon source, the Δ*lasR* strain obtained significantly reduced lag (*Figure 3B*) and higher yields (*Figure 3C*) than the wild type, and the enhanced growth phenotype was complementable by *lasR*. As previously reported, growth on phenylalanine depended on *cbrB*; the Δ*cbrB* and Δ*lasR*Δ*cbrB* mutants grew similarly poorly and their growth yield could be fully complemented by expressing *cbrB* (*Figure 3B and C*). Deletion of *crc* in the Δ*lasR*Δ*cbrB* strain also restored growth to levels comparable to the Δ*lasR* and Δ*lasR*Δ*cbrB*+*cbrB* strains (*Figure 3B and C*) indicating Crc repression of phenylalanine catabolism in the *cbrB* mutant. Overexpression of either *cbrB* or its target *crcZ*, which acts as a Crc-sequestering agent, was sufficient to improve yields on phenylalanine relative to the empty vector control (*Figure 3D*).

The CbrB- and Crc-controlled growth advantage on phenylalanine for LasR⁻ strains in planktonic cultures was also apparent in colony biofilms (*Figure 3—figure supplement 1A*). In colony biofilms, again, Δ*lasR* had improved growth on phenylalanine, that was dependent on *cbrB* and the growth defect of the *lasRcbrB* mutant could be rescued by deletion of *crc* (*Figure 3—figure supplement 1A*). The same pattern was observed on other substrates for which catabolism is under the control CbrAB-Crc pathway such as glucose and mannitol (*Figure 3—figure supplement 1A*). While deletion of *crc* was able to restore enhanced growth to the Δ*lasR*Δ*cbrB* mutant, Δ*crc* did not grow as robustly as the Δ*lasR* mutant which is consistent with the detection of LasR⁻ lineages but not Crc⁻ lineages in passaged wild type cultures. Thus, LasR⁻ strains from stationary phase cultures appear to be primed for growth on multiple single carbon sources under CbrB-Crc control and reach higher final yields on these substrates.

LasR⁻ strains have CbrB-dependent growth advantages on metabolites enriched in progressive cystic fibrosis lung infections

Loss-of-function mutations in *lasR* are commonly detected in samples from chronic *P. aeruginosa* lung infections in pwCF, and these mutants have been correlated with a more rapid rate in lung function decline (*Hoffman et al., 2009*). To determine the metabolite milieu in the CF lung, we performed a metabolomics analysis of bronchioalveolar lavage samples collected from 10 pwCF and 10 non-CF individuals (*Supplementary file 3*). The pwCF were infected with diverse pathogens and had varying lung function, which was measured as forced expiratory volume in 1 s and presented as the percent expected at one's age (%FEV$_1$). Over 300 compounds were measured, and no uniquely microbial metabolites were noted. Many compounds were higher in the CF population, but some were unchanged (e.g glucose) and others were higher in non-CF samples (e.g adenosine and glutathione as previously published *Esther et al., 2008*; *Fitzpatrick et al., 2014*; *Supplementary file 4*).

In a principal component analysis (PCA), samples from non-CF individuals clustered together while those from pwCF were more spread. Samples from pwCF with high lung function (112 or 113 %FEV$_1$) grouped among the non-CF samples (*Figure 4A*). The metabolites that contributed strongly to the first principal component, PC1, showed a significant inverse correlation with %FEV$_1$ including phenylalanine, arginine, lactate, and citrate (*Figure 4B*). As with phenylalanine (*Figure 3B and C* & *Figure 3—figure supplement 1A*), the Δ*lasR* strain had growth advantages on arginine, lactate, and citrate that were controlled by CbrB and Crc (*Figure 3—figure supplement 1A, B*).

We identified the 20 carbon sources that were most enriched in CF samples including those that correlated inversely with lung function, then used a BIOLOG phenotype array to assess whether the trend of greater yield for the Δ*lasR* strain persisted across this set. We found a significantly higher yield for the Δ*lasR* strain when we analyzed growth of the WT and Δ*lasR* across this group of 20 carbon sources suggesting that Δ*lasR* has improved growth on many of the nutrients available in the lung (*Figure 4C*).
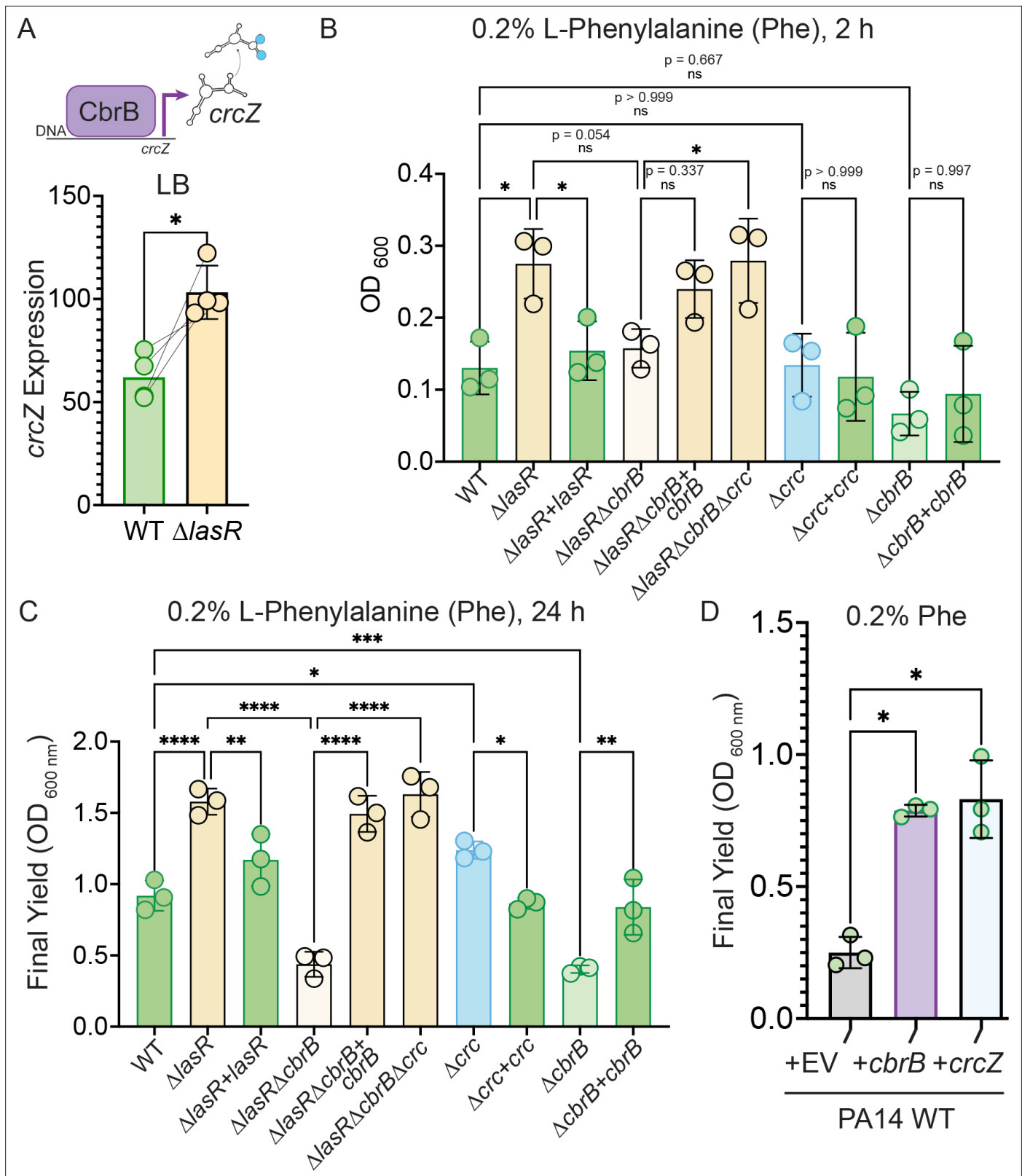
Figure 3. Increased CbrB activity of LasR⁻ strains is necessary and sufficient to promote growth on non-repressive substrates like phenylalanine via Crc. (**A**) CbrB promotes the transcription of *crcZ*, and *crcZ* thus can be a readout of CbrB transcriptional activity. *crcZ* expression was measured by qRT-PCR relative to the average expression of the housekeeping genes *rpoD* and *rpsL* in cultures of PA14 WT and Δ*lasR* strains grown to $OD_{600\,nm} = 1$ from four independent experiments. *, $p = 0.0334$ as determined by Student's paired two-tailed t-test. (**B**) Early growth (2 hr) and (**C**) Final yield (24 hr) on

Figure 3 continued on next page

Figure 3 continued

phenylalanine (Phe) as a sole carbon source shows enhanced growth for Δ*lasR, cbrB* dependence, and the requirement for *cbrB* is abolished by deletion of *crc*. Each point is the average of three replicates, repeated three independent days. Statistical significance determined by one-way ANOVA with Šídák's multiple comparisons test. ns, not significant. *, $p < 0.05$. **, $p < 0.005$. ****, $p < 0.0001$. (**D**) Final yield on Phe under (0.2%) arabinose-inducing conditions for the PA14 WT strain expressing an empty vector or *crcZ*, and *cbrB* overexpression constructs. Each point is the average of three replicates, performed on three separate days. Statistical significance determined by one-way ANOVA with multiple hypothesis correction as above.

The online version of this article includes the following figure supplement(s) for figure 3:

Figure supplement 1. Δ*lasR* strains have CbrB-dependent growth advantages that can be restored via loss of *crc*.

To further test the hypothesis that the growth phenotypes of LasR⁻ strains can promote selection in the nutrient environment of the CF lung, we performed evolution experiments using both strain PA14 and a LasR⁺ CF clinical isolate in a medium designed to more closely recapitulate the nutritional profile of the cystic fibrosis airway. Upon absolute quantitation, we observed good concordance between the relative abundances of amino acids found in BAL fluid and reported for sputum (*Palmer et al., 2005*) which served as a basis for an artificial sputum medium, ASM (*Figure 4—figure supplement 1*; *Clay et al., 2020*) that was based on a previously reported synthetic CF medium (SCFM2) (*Palmer et al., 2005*). LasR⁻ strains evolved in both strain backgrounds (*Figure 4D*) with kinetics similar to what was observed in LB medium (*Figure 1B*). Parallel evolution experiments in ASM initiated with Δ*cbrB* derivatives did not exhibit a rise in LasR⁻ phenotypes in either strain background to suggest that CbrAB activity was again a contributor to the fitness of *lasR* LOF mutants.

Discussion

Through mathematical modeling, experimental evolution, and competition assays, we found that the rise of problematic *P. aeruginosa* LasR⁻ variants frequently observed in disease could be explained by increases in yield and decreases in lag during growth on carbon sources abundant in the lung environment (*Figure 5*). In fact, the steady state growth rate for Δ*lasR* was slightly less than that for the wild type, which is consistent with the model that there are frequently tradeoffs between a shorter lag phase and overall growth rate (*Basan et al., 2020*). Interestingly, CF-adapted *P. aeruginosa* isolates have been found to have slower in vitro growth rates than other strains (*Yang et al., 2008*). Other factors will impact the relative fitness of LasR⁺ and LasR⁻ cells across different growth phases (*Figure 5*) including oxygen availability and pH buffering capacity, which may lead to differential lysis (*Heurlier et al., 2005*), or the need for (or exploitation of) proteases to gain access to growth substrates (*Van Delden et al., 1998*; *Sandoz et al., 2007*).

The overlap between the model-predicted and observed percentages of LasR⁻ strains over the course of the evolution regime suggests that the described social advantage resulting from QS dysfunction for LasR⁻ strains (i.e. social cheating) is not necessary to explain the timing and kinetics of the initial rise of LasR⁻ strains under our conditions. However, social interactions that benefit LasR-strains may be evident where the model estimates percentages that fall below or on the lower range of that experimentally observed, such as Day 4 or 6. A more detailed discussion of when social interactions are required is found below.

The data presented support the model that that increased growth of LasR⁻ cells on many amino acids, sugars, and lactate is due to higher CbrAB-controlled *crcZ* levels which downregulates metabolism under Crc control, and these findings nicely parallel studies by D'Argenio et al. (*D'Argenio et al., 2007*) that found higher levels of CbrB in LasR⁻ isolates. In PA14 Δ*cbrA* and Δ*cbrB* mutants, *lasR* LOF mutations did not arise, but mutations in *crc* and upstream of *hfq* were observed. As *crc* mutations phenocopy some of the growth advantages of the *lasR* mutants (*Figures 2C and 3*, *Figure 3—figure supplement 1*), the importance of derepressed catabolism for fitness is underscored. It is interesting to note that there were differences in the relative dependence on CbrB for the selection for LasR⁻ between strains PA14 and DH2417, and in ASM the dependence on *cbrB* for the selection of LasR⁻ strains increased in both strains (*Figure 4D*) suggesting that different environments may alter the importance of different LasR- and CbrB-controlled targets important for fitness that have yet to be elucidated. Though deletion of *cbrA* or *cbrB* can have pleiotropic effects (*Yeung et al., 2011*), we did not observe differences in density, quorum sensing regulation, production of quorum sensing controlled factors such as proteases, lysis in stationary phase, or overall mutation accumulation
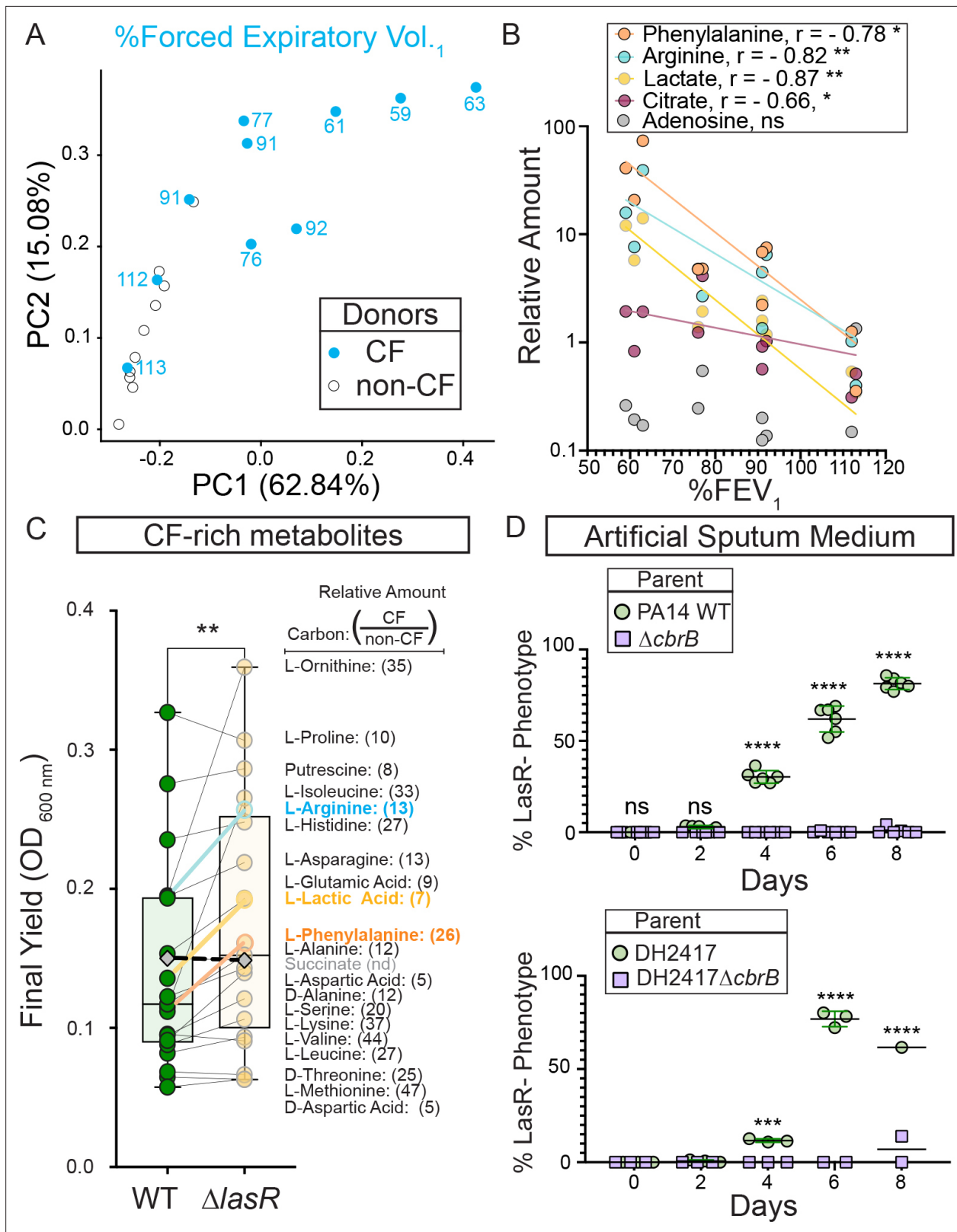
Figure 4. CbrB-dependent growth advantages may contribute to *lasR* mutant selection in distinct nutrient profiles of progressive cystic fibrosis airways. (**A**) The first two dimensions (PC1 and PC2) of a principal component analysis of log normalized metabolite counts from bronchoalveolar lavage (BAL) samples collected from cystic fibrosis (CF, blue filled) and non-cystic fibrosis (non-CF, gray open) donors explain 62.84% and 15.08% of the variation in the data, respectively. PC1 separates the metabolite data by relative lung function as measured by percent forced expiratory volume in 1 s (%FEV$_1$) for

Figure 4 continued on next page

Figure 4 continued

samples from people with CF. The %FEV₁ is overlayed for CF-donor samples with text. Samples from non-CF donors group more closely with CF-donor samples that have high lung function. (**B**) Spearman correlation analysis of the relative phenylalanine (orange), arginine (aqua), lactate (yellow), citrate (magenta), and adenosine (gray) metabolite counts in the BAL samples relative to %FEV₁ with exact p-values of 0.010, 0.005, 0.002, 0.041, and 0.714, respectively. Best fit semilog lines shown for visual clarity. (**C**) Comparison of the final yield measured after 24 hr for strains PA14 wild type and Δ*lasR* across a subset of carbon sources in BIOLOG growth assays for which the metabolite was found to be in higher abundance in CF-donor relative to non-CF donor BAL samples. Bold font indicates carbon sources analyzed in *Figure 3* and *Figure 3—figure supplement 1*. Number in parenthesis refers to the ratio of the average counts for each metabolite in CF relative to non-CF samples. **, p-value = 0.003 as determined by two-tailed paired t-test comparing growth across CF-enriched metabolites between the wild type and Δ*lasR* strains. Succinate (gray diamond, black dashed line) was not detected (nd) in the BAL samples and thus not included in the statistical analysis, but the growth data is shown for reference. (**D**) Observed percentage of colonies with LasR⁻ phenotypes over the course of evolution from strains (top) PA14 WT or (bottom) CF isolate (both green circles) with Δ*cbrB* (purple squares) derivatives in artificial sputum medium (ASM), which was designed to recapitulate the CF lung nutritional profile. ns, not significant (p-value > 0.9); ***, p = 0.0008; ****, p < 0.0001 as determined by ordinary two-way ANOVA with Šídák's multiple comparisons test.

The online version of this article includes the following figure supplement(s) for figure 4:

Figure supplement 1. Quantitative amino acid analysis.

between wild type, Δ*cbrA*, and Δ*cbrB* that could explain differences in the rise of LasR⁻ subpopulations. Furthermore, environmental modification of CbrB activity by the addition of succinate to LB (*Sonnleitner et al., 2009*) also suppressed the emergence of LasR⁻ strains in the wild type. Because CbrAB activity can still be suppressed by succinate in LasR⁻ cells (*Figure 2E*), LasR⁻ variants were not strictly 'de-repressed', and this is consistent with the fact that Δ*lasR* and Δ*crc* growth patterns were not identical. Unlike *lasR* mutations, *crc* mutations are not commonly observed in clinical isolates (*Winstanley et al., 2016*) and *crc* mutants have been shown to be under negative selection in Tn-Seq experiments (*Lorenz et al., 2019*).
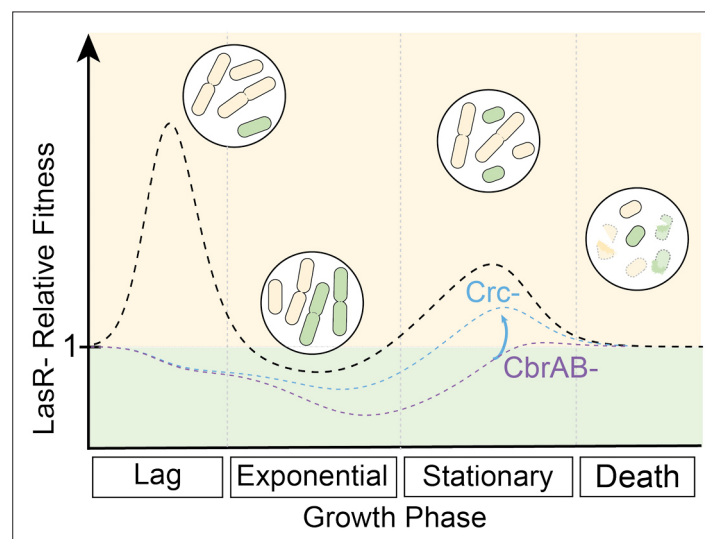

Figure 5. CbrAB activity contributes to the positive selection of LasR⁻ strains in complex media. LasR⁻ strain fitness relative to wild type is shown across growth phases, including lag, exponential growth, stationary, and death phases. Relative fitness of the LasR⁻ strain (dotted black line) is calculated from the experimentally determined monoculture growth data of strains PA14 wild type (WT) and Δ*lasR* over time. Values above one indicate a LasR⁻ strain fitness advantage over the WT strain during that growth phase. Circled insets show representative cartoons of LasR- (beige) and LasR+ (green) cells at each growth phase to indicate dividing or lysing cells (burst cells) across growth stages. The heights of the peaks or valleys of the relative fitness lines can be altered by several modulating factors including those that contribute to the positive and negative selection of LasR⁻ strains. Other modulating factors reported or suggested in the literature include inter- and intra- species competition, extracellular protease, immunoclearance, and oxygenation which are likely condition dependent. In the absence of CbrA or CbrB (CbrAB-, dotted purple line) or in the presence of succinate (one CbrAB repressive substrate), the relative growth of LasR⁻ strains is lower resulting in a reduction in the observed selection. This could be partially relieved in the CbrAB- background through disruption of Crc or Hfq function (blue dotted line), restoring activity through the pathway.

Analysis of BAL fluid revealed higher levels of substrates such as lactate and amino acids, which require CbrB for consumption, in samples from pwCF, and these findings are consistent with other more targeted analyses of CF airway samples (*Bensel et al., 2011*; *Twomey et al., 2013*). Consistent with our finding that higher levels of certain metabolites correlated with worse CF lung disease, other studies including that of *Esther et al., 2016* found a correlation between total metabolites and neutrophil counts suggesting host cell lysis, along with lysis of microbial cells, may be a major contributor to a shift in the metabolome. CF-lung derived *P. aeruginosa* isolates can have amino acid auxotrophies and enhanced amino acid uptake (*La Rosa et al., 2019*) which supports ready access to amino acids in vivo. Several CF isolates show reduced succinate assimilation to suggest the uptake of less preferred substrates over the course of adaptation, which may indicate decreased Crc activity over time (*Jørgensen et al., 2015*; *La Rosa et al., 2018*).

Our model predicts LasR⁻ strains benefit from growth advantages that might be present when new nutrients become available (analogous to lag phase) and in dense populations when improved yields for the ΔlasR mutant emerges; due to a slower steady state growth rate, we predict that LasR⁻ strains would not emerge under steady state growth conditions such as in a chemostat. Indeed, the advantages of decreased lag phase in cultures has been proposed to be a universal adaptation in dynamic environments (*Basan et al., 2020*; *Bertrand and Margolin, 2019*). Thus, the frequent emergence of LasR⁻ lineages in the CF lung and other disease settings suggests that *P. aeruginosa* often undergoes growth transitions in vivo, possibly due to fluctuating local conditions, spatial heterogeneity, or the result of complex competition between bacterial and host cell types. The CbrB-dependent rise of LasR⁻ strains in the complex CF mimetic medium (i.e. artificial sputum medium, ASM) alongside the positive selection observed in minimal media with CF relevant substrates (*Scribner et al., 2022*) shown to require CbrB for LasR⁻ strain growth enhancement suggests that the growth advantages of *lasR* mutants may be sufficient to overcome any potential negative selective pressures mediated by the host, neighboring microbes, or inaccessibility to nutrients like complex protein or adenosine. In addition, the loss of LasR function enables other inherent advantages that contribute to competitive fitness including resistance to lysis under conditions of high aeration, enhanced microoxic fitness, enhanced RhlR activity (*Chen et al., 2019*; *Clay et al., 2020*; *Heurlier et al., 2005*), and altered intraspecies interactions (*Mould et al., 2020*) which may be relevant in the complex and dynamic nutritional environment of the CF airway over the course of disease. The connection between these phenotypes and the CbrAB-*crcZ*-Crc pathway is not yet clear.

The increased growth in post-exponential phase cultures for LasR⁻ strains bears similarities to mutations that arise in other microbes. For example, the selection for *rpoS* mutants in stationary phase cultures of *E. coli* (*Finkel and Kolter, 1999*; *Zambrano et al., 1993*; *Zinser and Kolter, 2000*) is also dependent on nutrient accessibility (*Farrell and Finkel, 2003*) with enhanced amino acid catabolism as a major contributor to *E. coli* lineages with growth advantages in stationary phase (GASP) (*Zinser and Kolter, 1999*). While the rise of *rpoS* mutants in laboratory settings required pH-driven lysis (*Farrell and Finkel, 2003*), LasR⁻ strains still evolved in buffered medium suggesting distinct mechanisms for the metabolic advantages of *lasR* mutants. It is worth noting that none of the common GASP mutations (*rpoS, lrp,* or *ybeJ-gltJKL*) were identified in our in vitro evolution studies (*Supplementary file 1*). We considered that the enhanced growth of LasR⁻ strains in post-exponential growth phases may be due to differences in ppGpp signaling, given growth arrest as part of the stringent response modifies the expression of QS-regulated genes (*van Delden et al., 2001*). However, no mutations in *relA* or *spoT*, the two ppGpp synthases, were observed. The mechanism of increased CbrB activity in ΔlasR remains an unresolved question that is relevant to *P. aeruginosa* biology and may aid in the identification of the signals that activate the CbrA sensor kinase which influences clinically relevant phenotypes including virulence and antibiotic resistance (*Yeung et al., 2011*). Our working model is that the upregulation of CbrB transcription of *crcZ* increases levels of transporters and catabolic enzymes due to the release from Crc repression, and this enhanced substrate uptake alters intracellular metabolite pools driving metabolism in accordance with Le Chatelier's principle (*Monod, 1949*). Thus, quorum sensing mutants can maintain higher growth rates at lower substrate concentrations than for quorum-sensing intact cells.

The repeated observation that LOF mutations readily arise in diverse settings provokes the question of how quorum sensing is maintained. Several elegant mechanisms that address this point have been described. First, the wiring of the LasR regulon is such that while there are growth advantages

on many substrates present in the lung, there are growth disadvantages on other important nutrient sources (e.g. adenosine and proteins and peptides *Heurlier et al., 2005*). Social cheating can promote the rise of LOF mutants in protease-requiring environments (*Diggle et al., 2007*; *Hassett et al., 1999*). Second, there are quorum-sensing controlled 'policing' mechanisms through which LasR$^+$ strains restrict the growth of LasR$^-$ types through the release of products toxic to quorum-sensing mutants (*Castañeda-Tamez et al., 2018*; *García-Contreras et al., 2020*; *Wang et al., 2015*). Lastly, there are other tradeoffs such as sensitivity to oxidative stress that may limit LasR$^-$ lineage success (*Hassett et al., 1999*). Quorum sensing exerts metabolic control in other diverse microbes beyond *P. aeruginosa*. Thus, these data provide insight into generalizable explanations for the benefits of metabolic control in dense populations and indicate drivers for frequent loss-of-function mutations in quorum-sensing genes such as *agr* in *Staphylococcus aureus* and *hapR* in *Vibrio cholerae* (*Mould and Hogan, 2021*).

Together, these data highlight the power of coupling in vitro evolution studies with forward and reverse genetic analyses. Other benefits to this approach include the ability to dissect subtle differences between pathway components. For example, multiple mutations in *crc* repeatedly rose in Δ*cbrA*-, but not in Δ*cbrB*-derived populations, and multiple mutations in *hfq* rose in Δ*cbrB*-, and not in Δ*cbrA*-derived populations. While CbrA and B work together as do Crc and Hfq, these observations may provide a foothold into key distinctions that could yield mechanistic insights. In the future, the ability for deep sequencing of infection populations and analysis of evolutionary trajectories may aid diagnoses and treatment decisions in beneficial ways.

Materials and methods

See Key Resources Table in supplement for additional details on key reagents.

Strain construction and maintenance

In-frame deletions and complementation constructs were made using a *Saccharomyces cerevisiae* recombination technique described previously (*Shanks et al., 2006*). The *cbrB* and *crcZ* expression vectors were constructed by HiFi Gibson assembly with the NEBuilder HiFi DNA Assembly kit according to manufacturer's protocol. All plasmids were sequenced at the Molecular Biology Core at the Geisel School of Medicine at Dartmouth. In frame-deletion and complementation constructs were introduced into *P. aeruginosa* by conjugation via S17/lambda pir *E. coli*. Merodiploids were selected by drug resistance and double recombinants were obtained using sucrose counter-selection and genotype screening by PCR. Expression vectors were introduced into *P. aeruginosa* by electroporation and drug selection. All strains used in this study are listed in *Supplementary file 6*. Bacteria were maintained on lysogeny broth (LB) with 1.5% agar. Yeast strains for cloning were maintained on YPD (yeast extract-peptone-dextrose) with 2% agar. Artificial sputum medium (ASM) was made as described previously (*Clay et al., 2020*).

Mathematical model

Growth parameters were determined from 5 mL grown LB cultures inoculated as described in the experimental evolution protocol and the monocarbon growth below. In brief, a 16 h overnight LB culture was normalized to OD$_{600\,nm}$ = 1 in LB, and a 250 μL aliquot of the normalized culture was used to inoculate 5 mL fresh LB for an approximate OD$_{600\,nm}$ = 0.05 at time zero. The density (OD$_{600\,nm}$) was measured for up to 48 hr by taking a 10–100 μL aliquot at the designated time intervals from the 5 mL culture tube with dilution into LB as appropriate in a 96-well plate (100 μL total per well) for OD$_{600\,nm}$ measurement using a Spectramax M2 microplate reader with Softmax Pro 6.5.1 software. Lag and growth rate were measured in separate experiments from those used to monitor lysis so that the volume in the 5 mL cultures tubes never dropped below 10% of the starting volume. See *Supplementary file 7* for additional details for the parameter choices used in the mathematical model and *Source code 1* for the Matlab script.

Experimental evolution

Experimental evolution was modeled after work by *Heurlier et al., 2005*. A single colony of each strain was used to inoculate a 5 mL LB culture in 13 mm borosilicate tubes. The tubes inoculated with

a single colony were grown for 24 hr at 37 °C on a roller drum. The 24 hr grown culture was adjusted to $OD_{600 nm}$ = 1 in LB based on $OD_{600 nm}$ reading of a 1–10 dilution in LB of the 24 hr culture in a 1 cm cuvette using a Spectronic GENESYS 6 spectrophotometer. Separate 250 µL aliquots of the $OD_{600 nm}$ normalized cells was sub-cultured into three tubes containing 5 mL fresh media to initiate the evolution experiment (i.e. time 0) with three distinct replicate cultures per experiment. At time of passage every two days, 25 µL of culture was transferred into 5 mL fresh media. Every day (or as indicated) cultures were diluted and spread onto LB agar plates using sterile glass beads for phenotype distinction. The LB agar plates were incubated for ~ 24 hr at 37 °C and then left at room temperature for phenotype development. The sheen LasR⁻ colony morphologies were counted, and the percentage of LasR⁻ phenotypes calculated based on total CFUs. All experimental evolutions in LB were repeated on at least three independent days with three replicates of each strain per experiment unless otherwise stated. The ASM and succinate amended medium evolutions were completed on two separate days. In the case of ΔrhlR and Δanr, the three replicates were inoculated from three independent overnights. Data visualization and statistical analysis was performed in GraphPad Prism 9 (version 9.2.0).

gDNA extraction, sequencing, SNP calling of Pool-Seq data

Between 100 and 150 random colonies were scraped and pooled from the LB agar plates that were counted and used to measure the percent of colonies with LasR⁻ phenotypes at Days 4 and 6 from a representative WT-, ΔcrbA-, and ΔcbrB-initiated evolution experiment. For plates containing a total of 100–150 colonies, all colonies on the plate were collected for a single pooled genomic DNA extraction. If more than 150 colonies were on a plate, the plate was divided equally, and all colonies in an arbitrary section were collected to ensure genomic DNA was extracted from a similar number of colonies for each sample. Scraped up cells were pelleted briefly in a 1.5 mL Eppendorf tube via a short spin, resuspended in 1 mL PBS, vortexed briefly, and gDNA was subsequently extracted from a 50 µL aliquot of cell resuspension via the Master Pure Yeast DNA purification kit according to manufacturer's protocol with RNAase treatment. A 2.5 µg aliquot was submitted for Illumina sequencing (1Gbp) at the Microbial Genome Sequencing (MiGs) Center on the NextSeq 2000 platform. The resulting forward and reverse reads were trimmed with bcl2fastq (v2.20.0422) to remove Illumina adaptor sequences during the demultiplexing process. Both forward and reverse read files were aligned and compared to the complete and annotated UCBPP-PA14 genome available on NCBI (accession GCF_000014625.1) using the variant caller BreSeq (*Deatherage and Barrick, 2014*) (version 0.35.4) with the -p option for polymorphisms and a 5% cutoff. Specifically, the following command was used: breseq -p -j 10 r [reference file] [sample name]_.fastq.gz [sample name]_fastq.gz -o [output file name]. This provided an output file that specified variations from the reference genome and listed their respective fractions of the total reads. These fractions were treated as estimations of genotype proportions in the population. Variants at fixation (100%) across all 18 samples (three strains, 2 days) were excluded from follow-up analysis as potential differences in strain background that differed from the reference genome at the start of the experiment. All sequencing data is available on the Sequence Read Archive with the accession number PRJNA786588.

Milk proteolysis

Brain Heart Infusion Agar was supplemented with powdered skim milk dissolved in water to a final concentration of 1%. The evolved isolates selected on basis of 'sheen' colony morphology were grown in a 96-well plate with 200 µL LB per well for 16 hr. Milk plates were inoculated with ~ 5 µL of culture using a sterilized metal multiprong inoculation device (Dan-Kar) and incubated at 37 °C for 16 hr. PA14 WT and ΔlasR strains were included as controls. Colonies which showed a halo of clearing larger than the ΔlasR control strain were considered protease positive.

Acyl homoserine lactone autoinducer bioreporter assays

Protocol as described in *Mould et al., 2020*. Briefly, 100 µL of $OD_{600 nm}$ normalized LB overnight cultures ($OD_{600 nm}$ = 0.01) of the AHL-synthesis deficient reporter strains DH161 (3OC12HSL-specific) or DH162 (3OC12HSL or C4HSL responsive) with AHL-responsive promoters to *lacZ* (*Whiteley and Greenberg, 2001*; *Whiteley et al., 1999*) were bead spread on LB plates containing 150 µg/mL 5-bromo-4-chloro-3-indolyl-β-D-galactopyranoside (XGAL, dissolved in DMSO). Inoculated plates were allowed to dry 10 min in a sterile hood. Once dry, 5 µL of either the test strains or control cultures

(PA14 wild type and Δ*lasR* strains) were spotted onto the inoculated reporter lawns. After the spots dried, plates were incubated at 37 °C for 16 hr then stored at 4 °C to allow for further color development, if necessary, based on wild-type colony activity. The blue halo that formed around the colony was interpreted as AHL activity. The levels of AHL produced are approximated by the size of the blue halo formed around the colony.

Competition assays

Competition assays were performed by competing strains against an *att::lacZ* strain as previously reported (*Clay et al., 2020*). Overnight cultures of *att::lacZ* competitor and test strains were normalized to $OD_{600 \text{ nm}} = 1$ and mixed in the designated ratios with either a wild type control or Δ*lasR* strain. Aliquots of 10^{-6} dilutions of the initial mixed inoculums were immediately plated on LB plates containing 150 µg/mL XGAL by spreading an aliquot of 25–50 µL with sterilized glass beads. Roughly 100–200 colonies were counted to determine the initial ratios of PA14 *att:lacZ* to Δ*lasR* or the WT control strains by blue:white colony phenotype, respectively. To begin the competition experiment, a 250 µL aliquot of each undiluted mixed inoculum was sub-cultured into 5 mL fresh LB medium and incubated on a roller drum at 37 °C for 6 hr. After 6 hr, the cultures were collected, diluted by 10^{-6} in fresh liquid LB, and plated as previously stated for blue:white colony screening. The LB plates containing XGAL were incubated overnight at 37 °C prior to counting. Competitions were repeated on three separate days.

Kinase mutant evolution screen

Using an ethanol/flame sterilized metal multiprong inoculation device (Dan-Kar), the kinase mutant library (*Wang et al., 2021*) was inoculated into a 96-well plate with 200 µL LB per well for 24 hr shaking at 37 °C. The 24 hr grown cultures were used to inoculate two 96-well plates with each kinase mutant (including PA14 WT control) in triplicate. These cultures were grown for 48 hr upon which 2 µL was transferred to new 96 well plates with fresh 200 µL LB liquid per well. Every 2 days, the wells containing the wild-type replicates were diluted by 10^{-6} in fresh LB and 25 µL was bead spread onto LB for phenotypic distinction based on sheen colony morphology. At Day 14, when all wildtype replicates contained at least 50% LasR⁻ phenotypes, all wells were diluted and plated as stated previously for determination of sheen colony morphology. A secondary screen in 5 mL LB (as described above in Experimental Evolution section) was initiated with those mutant strains which did not show any LasR⁻ phenotypes across all three replicates in the microtiter assay at Day 14. The Circos plot summarizing the screen data was generated using BioCircos (*Cui et al., 2016*) in R (version 4.0.2) and re-colored in Adobe Illustrator.

Filtrate toxicity

Based on a protocol used previously (*Abisado et al., 2021*), strains were grown 16 hr in LB (5 mL) on a roller drum at 37 °C, centrifuged at 13 K RPM for 10 min in 2 mL aliquots, and the resulting supernatant was filter sterilized through a 0.22 µm pore filter. Per 5 mL filtrate, 250 µL of fresh LB was added. A 16 hr, grown LB culture (5 mL) of PA14 Δ*lasR* was normalized to an $OD_{600 \text{ nm}} = 1$ in LB, and 250 µL was used to inoculate 5 mL of the filtrate-LB mixture. The Δ*lasR* cultures were grown for 24 hr at 37 °C on the roller drum upon which colony counts were determined by bead spreading an appropriate dilution on LB plates. Data visualization and statistical analysis were performed in GraphPad Prism 9 (version 9.2.0).

Fluoroacetamide sensitivity assay

Strains were inoculated (either by patching from plates or by spotting 5 µL of 16 h LB grown culture) onto plates containing 1.5% agar with M63 salts,10 mM lactamide, and 40 mM succinate with or without 2.5 mg/mL filter-sterilized fluoroacetamide (FAA) dissolved in water based on protocol by *Collier et al., 2001*. Relative growth was compared in the presence and absence of FAA. PA14 wild type and Δ*crc* were included as controls in every experiment wherein wild type displays robust growth on FAA in the presence of succinate and the Δ*crc* strain, little to none.

Quantitative RT-PCR

The indicated strains were grown from single colonies in 5 mL LB cultures on a roller drum for 16 hr, normalized to an $OD_{600 \text{ nm}}$ of 1, and 250 µL of normalized culture was inoculated into 5 mL fresh LB for

a starting inoculum around $OD_{600\,nm} = 0.05$. The cultures were then grown at 37 °C on a roller drum until $OD_{600\,nm} = 1$ at which point a 1 mL aliquot of culture was pelleted by centrifugation for 10 min at 13 K RPM. Supernatant was removed, and the cell pellets were flash frozen in an ethanol dry ice bath. This was repeated on three separate days with one WT and one $\Delta lasR$ culture pair (n = 4) collected on each day or one $\Delta lasR$ and one $\Delta lasR\Delta cbrB$ culture pair (n = 3) each day. Pellets were stored at –80 °C until all sets of pellets were collected. RNA was extracted using the QIAGEN RNAeasy kit according to the manufacturer's protocol, and 7 µg RNA was twice DNAse treated with the Turbo DNA-free kit (Invitrogen). DNA contamination was checked by semi-quantitative PCR with gDNA standard for 35 cycles with *rpoD* qRT primers; if DNA contamination was greater than 0.004 ng / µL, the sample was DNAse treated again. cDNA was synthesized from 400 ng of DNase-treated RNA using the RevertAid H Minus first-strand cDNA synthesis kit (Thermo Scientific), according to the manufacturer's instructions for random hexamer primer (IDT) and a GC-rich template alongside an NRT control. Quantitative RT-PCR was performed on a CFX96 real-time system (Bio-Rad), using SsoFast Evergreen supermix (Bio-Rad) according to the following program: 95 °C for 30 s and 40 cycles of 95 °C for 5 s and 60 °C for 5 s followed by a melt curve with 65 °C for 3 s up to 95 °C in increments of 0.5 °C. Transcripts were normalized to the average *rpoD* and *rpsL* expression unless stated otherwise. *rpsL* and *crcZ* primers as designed in *Xia et al., 2020*. *rpoD* primers as designed in *Harty et al., 2019*. Data visualization and statistical analysis performed in GraphPad Prism 9 (version 9.2.0).

Mono-carbon growth

Single carbon sources were supplemented into M63 base (*Neidhardt et al., 1974*) and filter sterilized. A 16 hr overnight LB culture grown at 37 °C on a roller drum was normalized to an $OD_{600\,nm} = 1$ in 2 mL LB. For liquid growth curves, a 250 µL aliquot of the density adjusted culture was spiked into 5 mL fresh M63 medium with designated carbon source in triplicate, and growth was monitored using a Spectronic 20D+ (Spec20) hourly in 13 mm borosilicate tubes. Every point on the growth plots is the average of three replicates per day, repeated 3 days total. For colony biofilm growth, 5 µL of $OD_{600\,nm} = 1$ normalized culture was inoculated onto 1.5% agar plate of M63 medium containing the designated carbon source in singlicate and grown for 16 hr at 37 °C. Colonies were cored using the back of a P1000 tip and disrupted by 5 min on Genie Disrupter in 1 mL LB. Disrupted colony biofilms were serially diluted. 5 µL of the serial dilutions were plated and a 50 µL aliquot of diluted colony resuspension (10^{-6} or 10^{-7}-fold, depending on condition/strain) was bead spread and counted for colony forming units. Colony biofilm growth was assessed on >5 independent days. Data visualization and statistical analysis performed in GraphPad Prism 9 (version 9.2.0).

Metabolomics of bronchioloalveolar lavage fluid and artificial sputum medium

Human samples from people with and without cystic fibrosis were obtained with informed consent following institutional review board-approved protocols at Geisel School of Medicine at Dartmouth. The investigators were blinded to the conditions of the experiments during data collection and analysis. To obtain relative metabolite counts, bronchioloalveolar lavage (BAL) fluid samples were briefly centrifuged to exclude large debri then the supernatant was flash frozen in liquid nitrogen. Samples were processed by Metabolon via LC/MS for relative metabolite amounts. Raw values from Metabolon were normalized to protein concentrations by the BioRad Bradford protein concentration or raw area counts per day sample run and then the values were rescaled to set the median to one. Missing values were imputed with the minimum rescaled value for that biochemical. Quantitative amino acid concentrations were determined for aliquots of the same BAL samples (lyophilized) using the Biocrates AbsoluteIDQ p180 kit at the Duke Proteomics Core Facility. The lyophilized samples of BAL were homogenized in water and 50/50 water/methanol respectively to extract metabolites. 25 µL of the BAL extract were utilized for preparation of the samples on a Biocrates AbsoluteIDQ p180 plate. A Waters Xevo-TQ-S mass spectrometer was utilized to acquire targeted metabolite quantification on all samples and quality control specimens. Raw data (in µM) was exported independently for the FIA-MS/MS and UHPLC-MS/MS acquisition approaches used in this kit. The BAL sample data were corrected for the dilution factor since 25 µL was used versus 10 µL of the standards that were used to calculate the quantitative calibration curve. Principal component analysis of log normalized counts or concentrations were performed in R (version 4.0.2) (*R Development Core Team, 2021*) using the

prcomp() function and visualized with ggplot2 (*Wickham, 2016*) using ggfortify (*Tang et al., 2016*). *Supplementary file 3* of sample metadata was compiled with sjPlot (*Lüdecke, 2021*) in R.

BIOLOG phenotyping assay

Two mL of LB overnight cultures grown at 37 °C on a roller drum were washed twice with M63 salts with no carbon source by repeated centrifugation (10 min, 13 K RPM) and resuspension into fresh medium. The washed cultures were normalized to an $OD_{600\,nm}$ = 0.05 in 25 mL of fresh M63 salts base and 100 µL was used to resuspend dehydrated carbon sources on the bottom of PM1 and PM2 BIOLOG phenotype plates by repeated pipetting. Cells and resuspended carbon were transferred to a sterile flat bottom, black-walled 96 well plate and incubated at 37 °C, static. Every hour $OD_{600\,nm}$ was monitored in a plate reader for 24 hr. Endpoint (24 hr) data is reported. Data visualization and statistical analysis performed in GraphPad Prism 9 (version 9.2.0).

Additional information

Author contributions
Dallas L Mould, Conceptualization, Data curation, Formal analysis, Investigation, Methodology, Supervision, Validation, Visualization, Writing - original draft, Writing – review and editing; Mirjana Stevanovic, Formal analysis, Methodology, Writing – review and editing; Alix Ashare, Funding acquisition, Resources, Writing – review and editing; Daniel Schultz, Conceptualization, Formal analysis, Funding acquisition, Methodology, Supervision, Visualization, Writing – review and editing; Deborah A Hogan, Conceptualization, Formal analysis, Funding acquisition, Project administration, Supervision, Validation, Writing – review and editing

Author ORCIDs
Dallas L Mould ⬚ http://orcid.org/0000-0001-6939-1351
Deborah A Hogan ⬚ http://orcid.org/0000-0002-6366-2971

Decision letter and Author response
Decision letter https://doi.org/10.7554/eLife.76555.sa1
Author response https://doi.org/10.7554/eLife.76555.sa2

Additional files

Supplementary files
• Supplementary file 1. Unfixed mutations observed in Pool-Seq data from evolved populations. Fixed mutations (i.e. those mutations present at 100% across all samples at all time points) were excluded from this list as potential background differences from reference strain. All unfixed mutations are listed with unique mutation ID that consists of gene name, mutation position on the genome and the nature of the mutation. ‡ symbol indicates multiple changes within the same codon. Gene identifiers, gene name and product name indicated in Columns 2–5 (i.e. B - E) for each unique mutation ID. Columns 6 through 14 (i.e. F - N) represent the difference in the fractions of sequenced reads for the listed variants from Day 4 to Day 6 (i.e. Day 6 fraction - Day 4 fraction) for each strain and replicate. Columns 14 - end (i.e. N - AE) represent the fraction of the sequenced reads with the listed variant. Columns are labeled by gene knockout_day_replicate_fraction or change.

• Supplementary file 2. Evolution screen for spontaneous LasR- strains in kinase deletion mutant backgrounds. Number of replicates (three possible) with no LasR- phenotypes observed at time of plating in LB microtiter evolution assay for each clean deletion mutant. The locus tag, gene length, start and stop genomic position, gene name indicated were used to generate Circos plot shown in *Figure 2—figure supplement 1*. Deletion mutants that displayed no LasR- phenotypes across all three replicates were followed up in a secondary 5 mL LB evolution assay.

• Supplementary file 3. Bronchioalveolar lavage (BAL) fluid donor characteristics from people with and without cystic fibrosis (CF) used for metabolomics analyses. Samples are grouped according to CF status with non-CF donors denoted 'HV' with age group, gender, CFTR genotype, and percent forced expiratory volume in 1 s at the time of encounter listed. nd, not determined.

• Supplementary file 4. Relative metabolite counts in bronchioalveolar lavage fluid from people with cystic fibrosis (CF) and non-CF comparators by LC/MS. Values listed for each biochemical are normalized and imputed as described in the methods section. The percent forced expiratory volume in 1 s is noted for samples from people with CF as part of the column title. For Non-CF samples, column labels are listed numerically with 'Non-CF' indicator. Counts are shown per sample, as the average across CF (n = 10) and non-CF (n = 10) samples and as ratio of the averages between CF and non-CF as well. Information on (sub)pathway, biochemical identifiers, and methodology shown per biochemical.

• Supplementary file 5. Amino acid and biogenic amine concentrations in bronchioalveolar lavage (BAL) fluid from people with cystic fibrosis (CF) and non-CF comparators. Values listed are micromolar concentrations for specified metabolites quantified in the BAL samples from people with and without CF (non-CF) using the Biocrates AbsoluteIDQ p180 Kit (n = 10 and 2, respectively).

The percent forced expiratory volume in 1 s is noted for samples from people with CF as part of the column title. In addition to the concentrations listed per sample for each amino acid, the average is shown for samples from people with and without CF as well as a ratio of the averages.

• Supplementary file 6. Strains and plasmids used in this study. List of strains and plasmids used in this study with internal lab strain identifier, short description of strain/use including gene name and gene number, and source listed.

• Supplementary file 7. Supplemental methods for the choice of parameters for modeling wild type and LasR- frequencies in passaged cultures. Description of the terms for lag, growth, and death for both wild type strain PA14 and derived *lasR* mutants, and estimates of the number of *lasR* mutants in the initial population.

• Transparent reporting form

• Source code 1. Matlab script for deterministic mathematical model of LasR+ (wild type) strain PA14 and lasR mutant growth following density and percentage of each strain over the course of evolution regime as described in methods. Model parameters include growth rate, carrying capacity/concentration of saturated culture, killing rate (lysis-growth), difference in lag time (hours), and killing time at the end (hours) for each strain. Code output used to generate Figure 1A.

Data availability

All sequencing data is available on the Sequence Read Archive with accession number PRJNA786588 upon publication. All data generated or analyzed and all code used during this study are included in the manuscript or associated files.

The following dataset was generated:

Author(s)	Year	Dataset title	Dataset URL	Database and Identifier
Mould DL	2021	Pool Seq of Experimentally Evolved *P. aeruginosa* PA14 populations in LB	https://www.ncbi.nlm.nih.gov/sra/?term=PRJNA786588	NCBI Sequence Read Archive, PRJNA786588

References

Abisado RG, Kimbrough JH, McKee BM, Craddock VD, Smalley NE, Dandekar AA, Chandler JR. 2021. Tobramycin Adaptation Enhances Policing of Social Cheaters in *Pseudomonas aeruginosa. Applied and Environmental Microbiology* 87:e0002921. DOI: https://doi.org/10.1128/AEM.00029-21, PMID: 33837019

Basan M, Honda T, Christodoulou D, Hörl M, Chang Y-F, Leoncini E, Mukherjee A, Okano H, Taylor BR, Silverman JM, Sanchez C, Williamson JR, Paulsson J, Hwa T, Sauer U. 2020. A universal trade-off between growth and lag in fluctuating environments. *Nature* 584:470–474. DOI: https://doi.org/10.1038/s41586-020-2505-4, PMID: 32669712

Bensel T, Stotz M, Borneff-Lipp M, Wollschläger B, Wienke A, Taccetti G, Campana S, Meyer KC, Jensen PØ, Lechner U, Ulrich M, Döring G, Worlitzsch D. 2011. Lactate in cystic fibrosis sputum. *Journal of Cystic Fibrosis* 10:37–44. DOI: https://doi.org/10.1016/j.jcf.2010.09.004, PMID: 20947455

Bertrand RL, Margolin W. 2019. Lag Phase Is a Dynamic, Organized, Adaptive, and Evolvable Period That Prepares Bacteria for Cell Division. *Journal of Bacteriology* 201:e00618–e00697. DOI: https://doi.org/10.1128/JB.00697-18, PMID: 30642990

Boyle KE, Monaco HT, Deforet M, Yan J, Wang Z, Rhee K, Xavier JB. 2017. Metabolism and the Evolution of Social Behavior. *Molecular Biology and Evolution* 34:2367–2379. DOI: https://doi.org/10.1093/molbev/msx174, PMID: 28595344

Castañeda-Tamez P, Ramírez-Peris J, Pérez-Velázquez J, Kuttler C, Jalalimanesh A, Saucedo-Mora MÁ, Jiménez-Cortés JG, Maeda T, González Y, Tomás M, Wood TK, García-Contreras R. 2018. Pyocyanin Restricts Social Cheating in *Pseudomonas aeruginosa Frontiers in Microbiology* 9:1348. DOI: https://doi.org/10.3389/fmicb.2018.01348, PMID: 29997585

Chen R, Déziel E, Groleau MC, Schaefer AL, Greenberg EP. 2019. Social cheating in a *Pseudomonas aeruginosa* quorum-sensing variant. *PNAS* 116:7021–7026. DOI: https://doi.org/10.1073/pnas.1819801116, PMID: 30846553

Clay ME, Hammond JH, Zhong F, Chen X, Kowalski CH, Lee AJ, Porter MS, Hampton TH, Greene CS, Pletneva EV, Hogan DA. 2020. *Pseudomonas aeruginosa* lasR mutant fitness in microoxia is supported by an Anr-regulated oxygen-binding hemerythrin. *PNAS* 117:3167–3173. DOI: https://doi.org/10.1073/pnas.1917576117, PMID: 31980538

Collier DN, Spence C, Cox MJ, Phibbs PV. 2001. Isolation and phenotypic characterization of *Pseudomonas aeruginosa* pseudorevertants containing suppressors of the catabolite repression control-defective crc-10 allele. *FEMS Microbiology Letters* 196:87–92. DOI: https://doi.org/10.1111/j.1574-6968.2001.tb10546.x, PMID: 11267761

Crocker AW, Harty CE, Hammond JH, Willger SD, Salazar P, Botelho NJ, Jacobs NJ, Hogan DA. 2019. *Pseudomonas aeruginosa* Ethanol Oxidation by AdhA in Low-Oxygen Environments. *Journal of Bacteriology* **201**:23. DOI: https://doi.org/10.1128/JB.00393-19, PMID: 31527114

Cui Y, Chen X, Luo H, Fan Z, Luo J, He S, Yue H, Zhang P, Chen R. 2016. BioCircos.js: an interactive Circos JavaScript library for biological data visualization on web applications. *Bioinformatics (Oxford, England)* **32**:1740–1742. DOI: https://doi.org/10.1093/bioinformatics/btw041, PMID: 26819473

Deatherage DE, Barrick JE. 2014. Identification of mutations in laboratory-evolved microbes from next-generation sequencing data using breseq. *Methods in Molecular Biology (Clifton, N.J.)* **1151**:165–188. DOI: https://doi.org/10.1007/978-1-4939-0554-6_12, PMID: 24838886

Dettman JR, Sztepanacz JL, Kassen R. 2016. The properties of spontaneous mutations in the opportunistic pathogen *Pseudomonas aeruginosa*. *BMC Genomics* **17**:27. DOI: https://doi.org/10.1186/s12864-015-2244-3, PMID: 26732503

Diggle SP, Griffin AS, Campbell GS, West SA. 2007. Cooperation and conflict in quorum-sensing bacterial populations. *Nature* **450**:411–414. DOI: https://doi.org/10.1038/nature06279, PMID: 18004383

D'Argenio DA, Wu M, Hoffman LR, Kulasekara HD, Déziel E, Smith EE, Nguyen H, Ernst RK, Larson Freeman TJ, Spencer DH, Brittnacher M, Hayden HS, Selgrade S, Klausen M, Goodlett DR, Burns JL, Ramsey BW, Miller SI. 2007. Growth phenotypes of *Pseudomonas aeruginosa* lasR mutants adapted to the airways of cystic fibrosis patients. *Molecular Microbiology* **64**:512–533. DOI: https://doi.org/10.1111/j.1365-2958.2007.05678.x, PMID: 17493132

Esther CR, Alexis NE, Clas ML, Lazarowski ER, Donaldson SH, Ribeiro CMP, Moore CG, Davis SD, Boucher RC. 2008. Extracellular purines are biomarkers of neutrophilic airway inflammation. *The European Respiratory Journal* **31**:949–956. DOI: https://doi.org/10.1183/09031936.00089807, PMID: 18256064

Esther CR, Turkovic L, Rosenow T, Muhlebach MS, Boucher RC, Ranganathan S, Stick SM, AREST CF. 2016. Metabolomic biomarkers predictive of early structural lung disease in cystic fibrosis. *The European Respiratory Journal* **48**:1612–1621. DOI: https://doi.org/10.1183/13993003.00524-2016, PMID: 27836957

Farrell MJ, Finkel SE. 2003. The growth advantage in stationary-phase phenotype conferred by rpoS mutations is dependent on the pH and nutrient environment. *Journal of Bacteriology* **185**:7044–7052. DOI: https://doi.org/10.1128/JB.185.24.7044-7052.2003, PMID: 14645263

Feltner JB, Wolter DJ, Pope CE, Groleau MC, Smalley NE, Greenberg EP, Mayer-Hamblett N, Burns J, Déziel E, Hoffman LR, Dandekar AA. 2016. LasR Variant Cystic Fibrosis Isolates Reveal an Adaptable Quorum-Sensing Hierarchy in *Pseudomonas aeruginosa*. *MBio* **7**:e01516. DOI: https://doi.org/10.1128/mBio.01513-16, PMID: 27703072

Finkel SE, Kolter R. 1999. Evolution of microbial diversity during prolonged starvation. *PNAS* **96**:4023–4027. DOI: https://doi.org/10.1073/pnas.96.7.4023, PMID: 10097156

Fitzpatrick AM, Park Y, Brown LAS, Jones DP. 2014. Children with severe asthma have unique oxidative stress-associated metabolomic profiles. *The Journal of Allergy and Clinical Immunology* **133**:258–261. DOI: https://doi.org/10.1016/j.jaci.2013.10.012, PMID: 24369802

García-Contreras R, Loarca D. 2020. The bright side of social cheaters: potential beneficial roles of "social cheaters" in microbial communities. *FEMS Microbiology Ecology* **97**:fiaa239. DOI: https://doi.org/10.1093/femsec/fiaa239, PMID: 33238304

García-Contreras R, Loarca D, Pérez-González C, Jiménez-Cortés JG, Gonzalez-Valdez A, Soberón-Chávez G. 2020. Rhamnolipids stabilize quorum sensing mediated cooperation in *Pseudomonas aeruginosa*. *FEMS Microbiology Letters* **367**:fnaa080. DOI: https://doi.org/10.1093/femsle/fnaa080, PMID: 32407463

Groleau MC, Taillefer H, Vincent AT, Constant P, Déziel E. 2022. *Pseudomonas aeruginosa* isolates defective in function of the LasR quorum sensing regulator are frequent in diverse environmental niches. *Environmental Microbiology* **24**:1062–1075. DOI: https://doi.org/10.1111/1462-2920.15745, PMID: 34488244

Hammond JH, Hebert WP, Naimie A, Ray K, Van Gelder RD, DiGiandomenico A, Lalitha P, Srinivasan M, Acharya NR, Lietman T, Hogan DA, Zegans ME. 2016. Environmentally Endemic *Pseudomonas aeruginosa* Strains with Mutations in lasR Are Associated with Increased Disease Severity in Corneal Ulcers. *MSphere* **1**:e00140–e00116. DOI: https://doi.org/10.1128/mSphere.00140-16, PMID: 27631025

Harty CE, Martins D, Doing G, Mould DL, Clay ME, Occhipinti P, Nguyen D, Hogan DA. 2019. Ethanol Stimulates Trehalose Production through a SpoT-DksA-AlgU-Dependent Pathway in *Pseudomonas aeruginosa*. *Journal of Bacteriology* **201**:e00794–e00718. DOI: https://doi.org/10.1128/JB.00794-18, PMID: 30936375

Hassett DJ, Ma JF, Elkins JG, McDermott TR, Ochsner UA, West SE, Huang CT, Fredericks J, Burnett S, Stewart PS, McFeters G, Passador L, Iglewski BH. 1999. Quorum sensing in *Pseudomonas aeruginosa* controls expression of catalase and superoxide dismutase genes and mediates biofilm susceptibility to hydrogen peroxide. *Molecular Microbiology* **34**:1082–1093. DOI: https://doi.org/10.1046/j.1365-2958.1999.01672.x, PMID: 10594832

Heurlier K, Dénervaud V, Haenni M, Guy L, Krishnapillai V, Haas D. 2005. Quorum-sensing-negative (lasR) mutants of *Pseudomonas aeruginosa* avoid cell lysis and death. *Journal of Bacteriology* **187**:4875–4883. DOI: https://doi.org/10.1128/JB.187.14.4875-4883.2005, PMID: 15995202

Hoffman LR, Kulasekara HD, Emerson J, Houston LS, Burns JL, Ramsey BW, Miller SI. 2009. *Pseudomonas aeruginosa* lasR mutants are associated with cystic fibrosis lung disease progression. *Journal of Cystic Fibrosis* **8**:66–70. DOI: https://doi.org/10.1016/j.jcf.2008.09.006, PMID: 18974024

Jørgensen KM, Wassermann T, Johansen HK, Christiansen LE, Molin S, Høiby N, Ciofu Oana. 2015. Diversity of metabolic profiles of cystic fibrosis *Pseudomonas aeruginosa* during the early stages of lung infection. *Microbiology (Reading, England)* **161**:1447–1462. DOI: https://doi.org/10.1099/mic.0.000093, PMID: 25873584

La Rosa R, Johansen HK, Molin S. 2018. Convergent Metabolic Specialization through Distinct Evolutionary Paths in *Pseudomonas aeruginosa*. *MBio* **9**:e00269. DOI: https://doi.org/10.1128/mBio.00269-18, PMID: 29636437

La Rosa R, Johansen HK, Molin S. 2019. Adapting to the Airways: Metabolic Requirements of *Pseudomonas aeruginosa* during the Infection of Cystic Fibrosis Patients. *Metabolites* **9**:E234. DOI: https://doi.org/10.3390/metabo9100234, PMID: 31623245

LaFayette SL, Houle D, Beaudoin T, Wojewodka G, Radzioch D, Hoffman LR, Burns JL, Dandekar AA, Smalley NE, Chandler JR, Zlosnik JE, Speert DP, Bernier J, Matouk E, Brochiero E, Rousseau S, Nguyen D. 2015. Cystic fibrosis-adapted *Pseudomonas aeruginosa* quorum sensing *lasR* mutants cause hyperinflammatory responses. *Science Advances* **1**:e1500199. DOI: https://doi.org/10.1126/sciadv.1500199, PMID: 26457326

Lorenz A, Preuße M, Bruchmann S, Pawar V, Grahl N, Pils MC, Nolan LM, Filloux A, Weiss S, Häussler S. 2019. Importance of flagella in acute and chronic *Pseudomonas aeruginosa* infections. *Environmental Microbiology* **21**:883–897. DOI: https://doi.org/10.1111/1462-2920.14468, PMID: 30411474

Lüdecke D. 2021. sjPlot: Data Visualization for Statistics in Social Science (Version R package version 2.8.10) [SjPlot]. https://CRAN.R-project.org/package=sjPlot [Accessed November 26, 2021].

Luján AM, Moyano AJ, Segura I, Argaraña CE, Smania AM. 2007. Quorum-sensing-deficient (lasR) mutants emerge at high frequency from a *Pseudomonas aeruginosa* mutS strain. *Microbiology (Reading, England)* **153**:225–237. DOI: https://doi.org/10.1099/mic.0.29021-0, PMID: 17185551

McCready AR, Paczkowski JE, Henke BR, Bassler BL. 2019. Structural determinants driving homoserine lactone ligand selection in the *Pseudomonas aeruginosa* LasR quorum-sensing receptor. *PNAS* **116**:245–254. DOI: https://doi.org/10.1073/pnas.1817239116, PMID: 30559209

Monod J. 1949. THE GROWTH OF BACTERIAL CULTURES. *Annual Review of Microbiology* **3**:371–394. DOI: https://doi.org/10.1146/annurev.mi.03.100149.002103

Mould DL, Botelho NJ, Hogan DA. 2020. Intraspecies Signaling between Common Variants of *Pseudomonas aeruginosa* Increases Production of Quorum-Sensing-Controlled Virulence Factors. *MBio* **11**:e01865-20. DOI: https://doi.org/10.1128/mBio.01865-20, PMID: 32843558

Mould DL, Hogan DA. 2021. Intraspecies heterogeneity in microbial interactions. *Current Opinion in Microbiology* **62**:14–20. DOI: https://doi.org/10.1016/j.mib.2021.04.003, PMID: 34034081

Neidhardt FC, Bloch PL, Smith DF. 1974. Culture medium for enterobacteria. *Journal of Bacteriology* **119**:736–747. DOI: https://doi.org/10.1128/jb.119.3.736-747.1974, PMID: 4604283

O Brien S, Lujan AM, Paterson S, Cant MA, Buckling A. 2017. Adaptation to public goods cheats in *Pseudomonas aeruginosa*. *Proceedings. Biological Sciences* **284**:20171089. DOI: https://doi.org/10.1098/rspb.2017.1089, PMID: 28747481

Ozkaya O, Balbontín R, Gordo I, Xavier KB. 2018. Cheating on Cheaters Stabilizes Cooperation in *Pseudomonas aeruginosa*. *Current Biology* **28**:2070–2080. DOI: https://doi.org/10.1016/j.cub.2018.04.093, PMID: 30008329

O'Connor K, Zhao CY, Diggle SP. 2021. Frequency of Quorum Sensing Mutations in *Pseudomonas aeruginosa* Strains Isolated from Different Environments. *Microbiology* **1**:365. DOI: https://doi.org/10.1101/2021.02.22.432365

O'Toole GA, Gibbs KA, Hager PW, Phibbs PV, Kolter R. 2000. The global carbon metabolism regulator Crc is a component of a signal transduction pathway required for biofilm development by *Pseudomonas aeruginosa*. *Journal of Bacteriology* **182**:425–431. DOI: https://doi.org/10.1128/JB.182.2.425-431.2000, PMID: 10629189

Palmer KL, Mashburn LM, Singh PK, Whiteley M. 2005. Cystic fibrosis sputum supports growth and cues key aspects of *Pseudomonas aeruginosa* physiology. *Journal of Bacteriology* **187**:5267–5277. DOI: https://doi.org/10.1128/JB.187.15.5267-5277.2005, PMID: 16030221

Qi Q, Toll-Riera M, Heilbron K, Preston GM, MacLean RC. 2016. The genomic basis of adaptation to the fitness cost of rifampicin resistance in *Pseudomonas aeruginosa*. *Proceedings. Biological Sciences* **283**:1822. DOI: https://doi.org/10.1098/rspb.2015.2452, PMID: 26763710

R Development Core Team. 2021. R: A language and environment for statistical computing. 2.6.2. Vienna, Austria. R Foundation for Statistical Computing. https://www.R-project.org/

Robitaille S, Groleau MC, Déziel E. 2020. Swarming motility growth favours the emergence of a subpopulation of *Pseudomonas aeruginosa* quorum-sensing mutants. *Environmental Microbiology* **22**:2892–2906. DOI: https://doi.org/10.1111/1462-2920.15042, PMID: 32337826

Rodrigue A, Quentin Y, Lazdunski A, Méjean V, Foglino M. 2000. Two-component systems in *Pseudomonas aeruginosa*: why so many? *Trends in Microbiology* **8**:498–504. DOI: https://doi.org/10.1016/s0966-842x(00)01833-3, PMID: 11121759

Rumbaugh KP, Diggle SP, Watters CM, Ross-Gillespie A, Griffin AS, West SA. 2009. Quorum sensing and the social evolution of bacterial virulence. *Current Biology* **19**:341–345. DOI: https://doi.org/10.1016/j.cub.2009.01.050, PMID: 19230668

Sandoz KM, Mitzimberg SM, Schuster M. 2007. Social cheating in *Pseudomonas aeruginosa* quorum sensing. *PNAS* **104**:15876–15881. DOI: https://doi.org/10.1073/pnas.0705653104, PMID: 17898171

Schuster M, Lostroh CP, Ogi T, Greenberg EP. 2003. Identification, timing, and signal specificity of *Pseudomonas aeruginosa* quorum-controlled genes: a transcriptome analysis. *Journal of Bacteriology* **185**:2066–2079. DOI: https://doi.org/10.1128/JB.185.7.2066-2079.2003, PMID: 12644476

Schuster M, Greenberg EP. 2007. Early activation of quorum sensing in *Pseudomonas aeruginosa* reveals the architecture of a complex regulon. *BMC Genomics* **8**:287. DOI: https://doi.org/10.1186/1471-2164-8-287, PMID: 17714587

Scribner MR, Stephens AC, Huong JL, Richardson AR, Cooper VS. 2022. The Nutritional Environment Is Sufficient To Select Coexisting Biofilm and Quorum Sensing Mutants of *Pseudomonas aeruginosa*. *Journal of Bacteriology* **204**:e0044421. DOI: https://doi.org/10.1128/JB.00444-21, PMID: 34978461

Shanks RMQ, Caiazza NC, Hinsa SM, Toutain CM, O'Toole GA. 2006. *Saccharomyces cerevisiae* -Based Molecular Tool Kit for Manipulation of Genes from Gram-Negative Bacteria . *Applied and Environmental Microbiology* **72**:5027–5036. DOI: https://doi.org/10.1128/AEM.00682-06, PMID: 16820502

Smith EE, Buckley DG, Wu Z, Saenphimmachak C, Hoffman LR, D'Argenio DA, Miller SI, Ramsey BW, Speert DP, Moskowitz SM, Burns JL, Kaul R, Olson MV. 2006. Genetic adaptation by *Pseudomonas aeruginosa* to the airways of cystic fibrosis patients. *PNAS* **103**:8487–8492. DOI: https://doi.org/10.1073/pnas.0602138103, PMID: 16687478

Sonnleitner E, Abdou L, Haas D. 2009. Small RNA as global regulator of carbon catabolite repression in *Pseudomonas aeruginosa*. *PNAS* **106**:21866–21871. DOI: https://doi.org/10.1073/pnas.pnas.0910308106, PMID: 20080802

Sonnleitner E, Prindl K, Bläsi U. 2017. The *Pseudomonas aeruginosa* CrcZ RNA interferes with Hfq-mediated riboregulation. *PLOS ONE* **12**:e0180887. DOI: https://doi.org/10.1371/journal.pone.0180887, PMID: 28686727

Tang Y, Horikoshi M, Li W. 2016. ggfortify: Unified Interface to Visualize Statistical Results of Popular R Packages. *The R Journal* **8**:474. DOI: https://doi.org/10.32614/RJ-2016-060

Twomey KB, Alston M, An S-Q, O'Connell OJ, McCarthy Y, Swarbreck D, Febrer M, Dow JM, Plant BJ, Ryan RP. 2013. Microbiota and metabolite profiling reveal specific alterations in bacterial community structure and environment in the cystic fibrosis airway during exacerbation. *PLOS ONE* **8**:e82432. DOI: https://doi.org/10.1371/journal.pone.0082432, PMID: 24358183

Van Delden C, Pesci EC, Pearson JP, Iglewski BH. 1998. Starvation selection restores elastase and rhamnolipid production in a *Pseudomonas aeruginosa* quorum-sensing mutant. *Infection and Immunity* **66**:4499–4502. DOI: https://doi.org/10.1128/IAI.66.9.4499-4502.1998, PMID: 9712807

van Delden C, Comte R, Bally AM. 2001. Stringent response activates quorum sensing and modulates cell density-dependent gene expression in *Pseudomonas aeruginosa*. *Journal of Bacteriology* **183**:5376–5384. DOI: https://doi.org/10.1128/JB.183.18.5376-5384.2001, PMID: 11514523

Wang M, Schaefer AL, Dandekar AA, Greenberg Ep. 2015. Quorum sensing and policing of *Pseudomonas aeruginosa* social cheaters. *PNAS* **112**:2187–2191. DOI: https://doi.org/10.1073/pnas.1500704112, PMID: 25646454

Wang BX, Cady KC, Oyarce GC, Ribbeck K, Laub MT. 2021. Two-Component Signaling Systems Regulate Diverse Virulence-Associated Traits in *Pseudomonas aeruginosa*. *Applied and Environmental Microbiology* **87**:11. DOI: https://doi.org/10.1128/AEM.03089-20, PMID: 33771779

West SA, Griffin AS, Gardner A, Diggle SP. 2006. Social evolution theory for microorganisms. *Nature Reviews. Microbiology* **4**:597–607. DOI: https://doi.org/10.1038/nrmicro1461, PMID: 16845430

Whiteley M, Lee KM, Greenberg EP. 1999. Identification of genes controlled by quorum sensing in *Pseudomonas aeruginosa*. *PNAS* **96**:13904–13909. DOI: https://doi.org/10.1073/pnas.96.24.13904, PMID: 10570171

Whiteley M, Greenberg EP. 2001. Promoter specificity elements in *Pseudomonas aeruginosa* quorum-sensing-controlled genes. *Journal of Bacteriology* **183**:5529–5534. DOI: https://doi.org/10.1128/JB.183.19.5529-5534.2001, PMID: 11544214

Wickham H. 2016. *Ggplot2: Elegent Graphics for Data Analysis*. Cham: Springer-Verlag. DOI: https://doi.org/10.1007/978-3-319-24277-4

Winstanley C, O'Brien S, Brockhurst MA. 2016. *Pseudomonas aeruginosa* Evolutionary Adaptation and Diversification in Cystic Fibrosis Chronic Lung Infections. *Trends in Microbiology* **24**:327–337. DOI: https://doi.org/10.1016/j.tim.2016.01.008, PMID: 26946977

Wong A, Rodrigue N, Kassen R. 2012. Genomics of adaptation during experimental evolution of the opportunistic pathogen *Pseudomonas aeruginosa*. *PLOS Genetics* **8**:e1002928. DOI: https://doi.org/10.1371/journal.pgen.1002928, PMID: 23028345

Xia Y, Wang D, Pan X, Xia B, Weng Y, Long Y, Ren H, Zhou J, Jin Y, Bai F, Cheng Z, Jin S, Wu W. 2020. TpiA is a Key Metabolic Enzyme That Affects Virulence and Resistance to Aminoglycoside Antibiotics through CrcZ in *Pseudomonas aeruginosa*. *MBio* **11**:e02079. DOI: https://doi.org/10.1128/mBio.02079-19, PMID: 31911486

Yan H, Wang M, Sun F, Dandekar AA, Shen D, Li Na. 2018. A Metabolic Trade-Off Modulates Policing of Social Cheaters in Populations of *Pseudomonas aeruginosa Frontiers in Microbiology* **9**:337. DOI: https://doi.org/10.3389/fmicb.2018.00337, PMID: 29535700

Yang L, Haagensen JAJ, Jelsbak L, Johansen HK, Sternberg C, Høiby N, Molin S. 2008. In situ growth rates and biofilm development of *Pseudomonas aeruginosa* populations in chronic lung infections. *Journal of Bacteriology* **190**:2767–2776. DOI: https://doi.org/10.1128/JB.01581-07, PMID: 18156255

Yeung ATY, Bains M, Hancock REW. 2011. The sensor kinase CbrA is a global regulator that modulates metabolism, virulence, and antibiotic resistance in *Pseudomonas aeruginosa*. *Journal of Bacteriology* **193**:918–931. DOI: https://doi.org/10.1128/JB.00911-10, PMID: 21169488

Zambrano MM, Siegele DA, Almirón M, Tormo A, Kolter R. 1993. Microbial competition: *Escherichia coli* mutants that take over stationary phase cultures. *Science (New York, N.Y.)* **259**:1757–1760. DOI: https://doi.org/10.1126/science.7681219, PMID: 7681219

Zinser ER, Kolter R. 1999. Mutations enhancing amino acid catabolism confer a growth advantage in stationary phase. *Journal of Bacteriology* **181**:5800–5807. DOI: https://doi.org/10.1128/JB.181.18.5800-5807.1999, PMID: 10482523

Zinser ER, Kolter R. 2000. Prolonged stationary-phase incubation selects for lrp mutations in *Escherichia coli* K-12. *Journal of Bacteriology* **182**:4361–4365. DOI: https://doi.org/10.1128/JB.182.15.4361-4365.2000, PMID: 10894750

Appendix 1

Appendix 1—key resources table

Reagent type (species) or resource	Designation	Source or reference	Identifiers	Additional information
Gene (*Pseudomonas aeruginosa*)	PA14	NCBI	Accession: GCF_000014625.1	Reference file
Strain, strain background (*Saccharomyces cerevisiae*)	*Saccharomyces cerevisiae*	PMID:16820502		Cloning yeast
Strain, strain background (*Escherichia coli*)	DH5a	Invitrogen		Electrocompetent cells
Strain, strain background (*Escherichia coli*)	S17 λ pir	PMID:8226632		Electrocompetent cells made in lab
Strain, strain background (*P. aeruginosa*)	PA14 WT	PMID:7604262		Hogan Laboratory reference strain
Strain, strain background (*P. aeruginosa*)	DH2417; NC-AMT0101-1-2	PMID:16687478		Chronic CF lung infection isolate with functional LasR allele
Strain, strain background (*P. aeruginosa*)	PA14 WT	PMID:33771779		Laub Lab; strain background of kinase clean deletion mutants
Genetic reagent (*P. aeruginosa*)	PA14 Δ*lasR*	PMID:15554963		
Genetic reagent (*P. aeruginosa*)	PAO-MW1qsc102	PMID:10570171; PMID:11544214		AHL-sensing bioreporter; PAO1 *lasIrhlI* mutant with Tn5-B22, which contains promoterless *lacZ* located within PA1896 (hypothetical protein) at chromosomal location of 2,067,716. Responsive to $3OC_{12}$-HSL but not C_4-HSL.
Genetic reagent (*P. aeruginosa*)	PAO-MW1qsc131	PMID:10570171; PMID:11544214		AHL-sensing bioreporter; PAO1 *lasIrhlI* mutant with Tn5-B22, which contains promoterless *lacZ*, under *phzC* promoter control. Responsive to either $3OC_{12}$-HSL or C_4-HSL but requires both for full activation.
Genetic reagent (*P. aeruginosa*)	PA14 WT *att::lacZ*	PMID:31980538		PA14 WT with constitutive expression of *lacZ* for competition assays
Genetic reagent (*P. aeruginosa*)	PA14 Δ*cheA*	PMID:33771779		
Genetic reagent (*P. aeruginosa*)	PA14 Δ*chpA*	PMID:33771779		
Genetic reagent (*P. aeruginosa*)	PA14 Δ*creC*	PMID:33771779		
Genetic reagent (*P. aeruginosa*)	PA14 Δ*uhpB*	PMID:33771779		
Genetic reagent (*P. aeruginosa*)	PA14 Δ*bfiS*	PMID:33771779		
Genetic reagent (*P. aeruginosa*)	PA14 Δ*bphP*	PMID:33771779		
Genetic reagent (*P. aeruginosa*)	PA14 Δ*PA14_10770*	PMID:33771779		
Genetic reagent (*P. aeruginosa*)	PA14 Δ*PA14_11630*	PMID:33771779		

Appendix 1 Continued on next page

Appendix 1 Continued

Reagent type (species) or resource	Designation	Source or reference	Identifiers	Additional information
Genetic reagent (*P. aeruginosa*)	PA14 Δ*rocS1*	PMID:33771779		
Genetic reagent (*P. aeruginosa*)	PA14 Δ*narX*	PMID:33771779		
Genetic reagent (*P. aeruginosa*)	PA14 Δ*wspE*	PMID:33771779		
Genetic reagent (*P. aeruginosa*)	PA14 Δ*PA14_19340*	PMID:33771779		
Genetic reagent (*P. aeruginosa*)	PA14 Δ*mxtR*	PMID:33771779		
Genetic reagent (*P. aeruginosa*)	PA14 Δ*cpxS*	PMID:33771779		
Genetic reagent (*P. aeruginosa*)	PA14 Δ*gtrS*	PMID:33771779		
Genetic reagent (*P. aeruginosa*)	PA14 Δ*PA14_24340*	PMID:33771779		
Genetic reagent (*P. aeruginosa*)	PA14 Δ*rocS2*	PMID:33771779		
Genetic reagent (*P. aeruginosa*)	PA14 Δ*PA14_26810*	PMID:33771779		
Genetic reagent (*P. aeruginosa*)	PA14 Δ*sagS*	PMID:33771779		
Genetic reagent (*P. aeruginosa*)	PA14 Δ*copS*	PMID:33771779		
Genetic reagent (*P. aeruginosa*)	PA14 Δ*pfeS*	PMID:33771779		
Genetic reagent (*P. aeruginosa*)	PA14 Δ*bqsS*	PMID:33771779		
Genetic reagent (*P. aeruginosa*)	PA14 Δ*PA14_30700*	PMID:33771779		
Genetic reagent (*P. aeruginosa*)	PA14 Δ*PA14_30840*	PMID:33771779		
Genetic reagent (*P. aeruginosa*)	PA14 Δ*czcS*	PMID:33771779		
Genetic reagent (*P. aeruginosa*)	PA14 Δ*PA14_32570*	PMID:33771779		
Genetic reagent (*P. aeruginosa*)	PA14 Δ*PA14_36420*	PMID:33771779		
Genetic reagent (*P. aeruginosa*)	PA14 Δ*ercS*	PMID:33771779		
Genetic reagent (*P. aeruginosa*)	PA14 Δ*exaD*	PMID:33771779		
Genetic reagent (*P. aeruginosa*)	PA14 Δ*ercS'*	PMID:33771779		
Genetic reagent (*P. aeruginosa*)	PA14 Δ*parS*	PMID:33771779		
Genetic reagent (*P. aeruginosa*)	PA14 Δ*kdpD*	PMID:33771779		
Genetic reagent (*P. aeruginosa*)	PA14 Δ*PA14_43670*	PMID:33771779		

Appendix 1 Continued on next page

Appendix 1 Continued

Reagent type (species) or resource	Designation	Source or reference	Identifiers	Additional information
Genetic reagent (*P. aeruginosa*)	PA14 ΔPA14_45590	PMID:33771779		
Genetic reagent (*P. aeruginosa*)	PA14 ΔPA14_45870	PMID:33771779		
Genetic reagent (*P. aeruginosa*)	PA14 ΔPA14_46370	PMID:33771779		
Genetic reagent (*P. aeruginosa*)	PA14 ΔPA14_46980	PMID:33771779		
Genetic reagent (*P. aeruginosa*)	PA14 ΔPA14_48160	PMID:33771779		
Genetic reagent (*P. aeruginosa*)	PA14 Δ*phoQ*	PMID:33771779		
Genetic reagent (*P. aeruginosa*)	PA14 ΔPA14_49420	PMID:33771779		
Genetic reagent (*P. aeruginosa*)	PA14 Δ*fleS*	PMID:33771779		
Genetic reagent (*P. aeruginosa*)	PA14 Δ*pirS*	PMID:33771779		
Genetic reagent (*P. aeruginosa*)	PA14 Δ*gacS*	PMID:33771779		
Genetic reagent (*P. aeruginosa*)	PA14 Δ*tctE*	PMID:33771779		
Genetic reagent (*P. aeruginosa*)	PA14 Δ*pprA*	PMID:33771779		
Genetic reagent (*P. aeruginosa*)	PA14 Δ*colS*	PMID:33771779		
Genetic reagent (*P. aeruginosa*)	PA14 ΔPA14_57170	PMID:33771779		
Genetic reagent (*P. aeruginosa*)	PA14 Δ*roxS*	PMID:33771779		
Genetic reagent (*P. aeruginosa*)	PA14 Δ*rcsC*	PMID:33771779		
Genetic reagent (*P. aeruginosa*)	PA14 Δ*pvrS*	PMID:33771779		
Genetic reagent (*P. aeruginosa*)	PA14 Δ*pilS*	PMID:33771779		
Genetic reagent (*P. aeruginosa*)	PA14 Δ*cbrA*	PMID:33771779		
Genetic reagent (*P. aeruginosa*)	PA14 Δ*pmrB*	PMID:33771779		
Genetic reagent (*P. aeruginosa*)	PA14 Δ*retS*	PMID:33771779		
Genetic reagent (*P. aeruginosa*)	PA14 ΔPA14_64580	PMID:33771779		
Genetic reagent (*P. aeruginosa*)	PA14 Δ*aruS*	PMID:33771779		
Genetic reagent (*P. aeruginosa*)	PA14 Δ*ntrB*	PMID:33771779		
Genetic reagent (*P. aeruginosa*)	PA14 ΔPA14_68230	PMID:33771779		

Appendix 1 Continued

Reagent type (species) or resource	Designation	Source or reference	Identifiers	Additional information
Genetic reagent (*P. aeruginosa*)	PA14 Δ*amgS*	PMID:33771779		
Genetic reagent (*P. aeruginosa*)	PA14 Δ*algZ*	PMID:33771779		
Genetic reagent (*P. aeruginosa*)	PA14 Δ*phoR*	PMID:33771779		
Genetic reagent (*P. aeruginosa*)	PA14 Δ*kinB*	PMID:33771779		
Genetic reagent (*P. aeruginosa*)	PA14 ΔPA14_72740	PMID:33771779		
Genetic reagent (*P. aeruginosa*)	PA14 Δ*rhlR*	PMID:30936375		
Genetic reagent (*P. aeruginosa*)	PA14 Δ*anr*	PMID:31527114		
Genetic reagent (*P. aeruginosa*)	PA14 Δ*cbrB*	This paper		PA14 WT with in-frame deletion of *cbrB* (PA14_62540)
Genetic reagent (*P. aeruginosa*)	PA14 *cbrB*::Tn*M*	PMID:22911607; PMID:16477005		*cbrB* MAR2xT7 transposon insertion mutant
Genetic reagent (*P. aeruginosa*)	DH2417Δ*cbrB*; NC-AMT0101-1-2Δ*cbrB*	This paper		CF clinical isolate NC-AMT0101-1-2 (DH2417) with in-frame deletion of *cbrB* (PA14_62540)
Genetic reagent (*P. aeruginosa*)	PA14 Δ*crc*	This paper		PA14 WT with in-frame deletion of *crc* (PA14_70390)
Genetic reagent (*P. aeruginosa*)	PA14 Δ*crc* + *crc*	This paper		PA14 Δ*crc* with complementation of *crc* (PA14_70390) at the native locus
Genetic reagent (*P. aeruginosa*)	PA14 Δ*lasR* + *lasR*	PMID:31980538		
Genetic reagent (*P. aeruginosa*)	PA14 Δ*cbrB* + pMQ70 *cbrB* (plasmid)	This paper		PA14 Δ*cbrB* expressing arabinose inducible pMQ70 *cbrB* expression vector
Genetic reagent (*P. aeruginosa*)	PA14 Δ*lasR*Δ*cbrB*	This paper		PA14 Δ*lasR* with in-frame deletion of *cbrB* (PA14_62540)
Genetic reagent (*P. aeruginosa*)	PA14 Δ*lasR*Δ*cbrB* + *cbrB*	This paper		PA14 Δ*lasR*Δ*cbrB* with complementation of *cbrB* (PA14_62540) at the native locus
Genetic reagent (*P. aeruginosa*)	PA14 Δ*lasR*Δ*cbrB*Δ*crc*	This paper		PA14 Δ*lasR*Δ*cbrB* with in-frame deletion of *crc* (PA14_70390)
Genetic reagent (*P. aeruginosa*)	PA14 Δ*lasR*Δ*crc*	This paper		PA14 Δ*lasR* with in-frame deletion of *crc* (PA14_70390)
Genetic reagent (*P. aeruginosa*)	PA14 Δ*lasR*Δ*crc* + *crc*	This paper		PA14 Δ*lasR*Δ*crc* with complementation of *crc* (PA14_70390) at the native locus
Genetic reagent (*P. aeruginosa*)	PA14 + pMQ72 EV	This paper		PA14 WT expressing pMQ72 empty vector
Genetic reagent (*P. aeruginosa*)	PA14 + pMQ70 *cbrB*	This paper		PA14 WT expressing arabinose inducible pMQ70 *cbrB* expression vector
Genetic reagent (*P. aeruginosa*)	PA14 + pMQ72 *crcZ*	This paper		PA14 WT expressing arabinose inducible pMQ72 *crcZ* expression vector
Recombinant DNA reagent	pMQ30 EV	PMID:16820502		
Recombinant DNA reagent	pMQ72 EV	PMID:16820502		
Recombinant DNA reagent	pMQ70 EV	PMID:16820502		

Appendix 1 Continued on next page

Appendix 1 Continued

Reagent type (species) or resource	Designation	Source or reference	Identifiers	Additional information
Recombinant DNA reagent	pMQ30_*cbrB*_KO	This paper		pMQ30 plasmid for knocking out *cbrb*
Recombinant DNA reagent	pMQ30_*crc*_KO	This paper		pMQ30 plasmid for knocking out *crc*
Recombinant DNA reagent	pMQ30_*cbrB*_KON	This paper		pMQ30 plasmid for complementing *cbrb* at the native locus
Recombinant DNA reagent	pMQ30_*crc*_KON	This paper		pMQ30 plasmid for complementing *cbrb* at the native locus
Recombinant DNA reagent	pMQ72_*crcZ*	This paper		pMQ72 plasmid backbone with arabinose inducible *crcZ* expression
Recombinant DNA reagent	pMQ70_*cbrB*	This paper		pMQ70 plasmid backbone with arabinose inducible *cbrB* expression
Sequence-based reagent	pMQ72 crcZ OE 1 F	This paper	PCR Primers; construct design	gtttctccatacccgtttttttgggctagcGCACAACAACAATAACAAGCAACGACGAAG
Sequence-based reagent	pMQ72 crcZ OE 2 R	This paper	PCR Primers; construct design	ctagaggatccccgggtaccgagctcgaattcgaaatggtgtaaggcgaaggaaaaacgg
Sequence-based reagent	pMQ70 *cbrB* OE 1 F	This paper	PCR Primers; construct design	ctctctactgtttctccatacccgtttttttgggctagcgAGACGAGCgaattcACGTCGAGAGAGCtgaatacatggcac
Sequence-based reagent	pMQ70 *cbrB* OE 2 R	This paper	PCR Primers; construct design	ttgcatgcctgcaggtcgactctagaggatccccgggtacGTAACAGGTTGCAGGGTaccGTtacgagtcggccgaggcccc
Sequence-based reagent	pMQ30 *cbrB* KO 1 F	This paper	PCR Primers; construct design	taacaatttcacacaggaaacagctatgaccatgattacgaattcAGGAAGTGCTGATGTGGAACC
Sequence-based reagent	pMQ30 *cbrB* KO 2 R	This paper	PCR Primers; construct design	GTAACAGGTTGCAGGGTGTTTATTCAGCTCTCTCGACGTGCT
Sequence-based reagent	pMQ30 *cbrB* KO 3 F	This paper	PCR Primers; construct design	CACGTCGAGAGAGCTGAATAAACACCCTGCAACCTGTTACC
Sequence-based reagent	pMQ30 *cbrB* KO 4 R	This paper	PCR Primers; construct design	aggtcgactctagaggatccccgggtaccgagctcgaattcCAGGGAGTGCTGGTTGTTACCGATGACTtc
Sequence-based reagent	pMQ30 *crc* KO 1 F	This paper	PCR Primers; construct design	taacaatttcacacaggaaacagctatgaccatgattacgaattcTGGAATACAGGCGCAGCAac
Sequence-based reagent	pMQ30 *crc* KO 2 R	This paper	PCR Primers; construct design	TAGAAAAGCCGGCGCATGCGCTGGCTTTTTCGTGTCTGACGGGGCAAATGGCCCCCAAAATCACGTGCG
Sequence-based reagent	pMQ30 *crc* KO 4 R	This paper	PCR Primers; construct design	ctgcaggtcgactctagaggatccccgggtaccgagctcgaattcttggctgaccgccgagtacggcatgc
Sequence-based reagent	pMQ30 *crc* KO 3 F	This paper	PCR Primers; construct design	TTTGAGCTCGGGTATCATACACGCACGTGATTTTGGGGGCCATTTGCCCCGTCAGACACGAAAAAGCCAG
Sequence-based reagent	*cbrB* check F	This paper	PCR primer, KO check	GCGTCTGCTCCCTGGCCAAG
Sequence-based reagent	*cbrB* check R	This paper	PCR primer, KO check	GTGGCGCTGGTGGCGACATC
Sequence-based reagent	*crc* check F	This paper	PCR primer, KO check	GCTCGATGGCGAAACGAATG
Sequence-based reagent	*crc* check R	This paper	PCR primer, KO check	GCGCTGGTGTTGACCATCATC
Sequence-based reagent	crcZ RT 1 F	PMID:31911486	PCR Primers	GCACAACAACAATAACAAGCAACG
Sequence-based reagent	crcZ RT 2 R	PMID:31911486	PCR Primers	AGTTTTATTCTTCTTCCGACTGGCT

Appendix 1 Continued on next page

Appendix 1 Continued

Reagent type (species) or resource	Designation	Source or reference	Identifiers	Additional information
Sequence-based reagent	rpsL RT1F	PMID:31911486	PCR Primers	GTAAGGTATGCCGTGTACG
Sequence-based reagent	rpsL RT 2 R	PMID:31911486	PCR Primers	CACTACGCTGTGCTCTTG
Sequence-based reagent	rpoD RT 1 F	PMID:30936375	PCR Primers	CGCCGAGATCAAGGAAATCA
Sequence-based reagent	rpoD RT 2 R	PMID:30936375	PCR Primers	TACTTCTTGGCGATGGAAATCA
Commercial assay, kit	NEBuilder HiFi DNA Assembly	Biolabs	Cat. #: E2621L	Gibson cloning
Commercial assay, kit	Master Pure Yeast DNA purification kit	Lucigen	Cat. No.: MPY80200	
Commercial assay, kit	RNAeasy Mini kit	QIAGEN	Cat. No.: 74,104	
Commercial assay, kit	Turbo DNA-free kit	Thermo Fisher Scientific	AM1907	
Commercial assay, kit	RevertAid H Minus First Strand cDNA synthesis	Thermo Scientific	Cat. No.: EP0451	cDNA synthesis with IDT random hexamer
Commercial assay, kit	SsoFast EvaGreen Supermix	BIO-RAD	Cat.#: 1725201	
Commercial assay, kit	Zymoprep Yeast Plasmid Miniprep II	Zymo Research	Cat. No.: D2004	Yeast cloning
Commercial assay, kit	Biocrates AbsoluteIDQ p180 kit	biocrates		Amino acid. quantification
Chemical compound, drug	Brain Heart Infusion	BD	SKU:211,059	BBL Brain Heart Infusion
Chemical compound, drug	Agar	BD	SKU:214,510	Difco Agar, granulated (2 Kg pail)
Chemical compound, drug	XGAL; 5-bromo-4-chloro-3-indolyl-β-D-galactopyranoside	Research Products International	B71800-5.0	Stock dissolved in DMSO
Chemical compound, drug	Fluoroacetamide	Aldrich	128341–5 G	dissolved in water, filter sterilized
Chemical compound, drug	Lactamide	Tokyo Chemical Industry	Product Number: L0001	
Chemical compound, drug	Mannitol	Sigma	M8429-500G	D-Mannitol
Chemical compound, drug	Succinate	Sigma	S9512-500G	Succinic acid, to pH7 with NaOH
Chemical compound, drug	Phenylalanine	Sigma-Aldrich	P2126-100G	L-Phenylalanine
Chemical compound, drug	Arginine	Sigma	A5131-100G	L-arginine monohydrochloride
Chemical compound, drug	Lactate	Fisher Scientific	S326-500	Sodium lactate syrup, 60% w/w
Chemical compound, drug	Glucose	VWR Chemicals	BDH9230-2.5KG	Dextrose, anhydrous
Chemical compound, drug	Citrate	FisherScientific	A104-500	Citric acid, monohydrate

Appendix 1 Continued

Reagent type (species) or resource	Designation	Source or reference	Identifiers	Additional information
Chemical compound, drug	Gentamicin	Research Products International	G38000-10.0	Gentamicin Sulfate
Chemical compound, drug	Nalidixic acid	Research Products International	N42000-25.0	
Chemical compound, drug	Carbinicillin	Goldbio	C-103–25	Carbenicillin (Disodium)
Chemical compound, drug	Sucrose	Fisher BioReagents	BP220-212; 2.5 kg	D-Sucrose
Chemical compound, drug	HEPES	SIGMA	H3375-100G	buffer
Chemical compound, drug	Tryptone	Fisher Bioreagents	BP1421-500	LB
Chemical compound, drug	NaCl; sodium chloride	Fisher Chemical	S271-3	LB
Chemical compound, drug	Yeast extract	Fisher Bioreagents	BP1422-500	LB
Chemical compound, drug	Ammonium sulfate	Fisher Chemical	A702-500	M63
Chemical compound, drug	Potassium phosphate monobasic	Fisher Chemical	P382-500	M63
Chemical compound, drug	Potassium phosphate dibasic, anhydrous	Fisher Chemical	P288-500	M63
Chemical compound, drug	Magnesium Sulfate	Fisher Scientific	M63-500	M63
Chemical compound, drug	Milk	BD	232,100	Difco Skim Milk
Chemical compound, drug	Yeast Nitrogen Base without amino acids	Research Products International	Y20040-500.0	Yeast cloning
Chemical compound, drug	Yeast Synthetic Drop-out Medium Supplements without uracil	Sigma	Y1501-20G	Yeast cloning
Chemical compound, drug	Peptone	Fisher bioreagents	BP1420-500	YPD
Chemical compound, drug	Sodium phosphate dibasic anhydrous	Fisher Chemicals	S374-500	ASM
Chemical compound, drug	Sodium phosphate monobasic	Fisher Chemicals	S369-500	ASM
Chemical compound, drug	Potassium Nitrate	Fisher Chemicals	M-12636	ASM
Chemical compound, drug	Potassium Sulfate	Fisher Chemicals	P304-500	ASM
Chemical compound, drug	L-(+)-Lactic acid	Sigma	L1750-10G	ASM; 1 M stock; pH to 7 with NaOH
Chemical compound, drug	Calcium chloride dihydrate	Sigma	C7902-500G	ASM
Chemical compound, drug	Magnesium Chloride Hexahydrate	Fisher chemical	M33-500	ASM

Appendix 1 Continued on next page

Appendix 1 Continued

Reagent type (species) or resource	Designation	Source or reference	Identifiers	Additional information
Chemical compound, drug	FeSO$_4$*7H$_2$O	Sigma-Aldrich	F-8048	ASM; Ferrous sulfate heptahydrate; Filter sterilized
Chemical compound, drug	N-acetylglucosamine	Fisher Scientific	AAA1304718	ASM
Chemical compound, drug	DPPC	Sigma	P0763-250MG	ASM; 1,2-dipalmitoyl-sn-glycero-3-phosphocholine; dissolved in chloroform
Chemical compound, drug	Tryptophan	Sigma-Aldrich	T0254-25G	ASM, L-Tryptophan
Chemical compound, drug	Mucin	Sigma	M2378-100G	ASM; Mucin from porcine stomach, Type II
Peptide, recombinant protein	Phusion	New England BioLabs	M0530L	High-Fidelity DNA polymerase
Software, algorithm	MATLAB	MathWorks		
Software, algorithm	breseq	PMID:24838886		Version 0.35.4
Software, algorithm	bcl2fastq	Illumina	RRID:SCR_015058	v2.20.0422
Software, algorithm	GraphPad Prism 9	GraphPad		Version 9.2.0